ANALYSIS OF MIXED CONVECTION IN AN AIR FILLED SQUARE CAVITY

A dissertation submitted to the University of KwaZulu-Natal

for the degree of Master of Science

in the Faculty of Science & Agriculture

By

Deborah S Ducasse

School of Mathematical Sciences

September 2010

Contents

List of Figures

Abstract

A steady state two-dimensional mixed convection problem in an air filled square unit cavity has been numerically investigated. Two different cases of heating are investigated and compared. In the first case, the bottom wall was uniformly heated, the side walls were linearly heated and the top moving wall was heated sinusoidally. The second case differed from the first in that the side walls were instead uniformly cooled. This investigation is an extension of the work by Basak et al. [6, 7] who investigated mixed convection in a square cavity with similar boundary conditions to the cases listed above with the exception of the top wall which was well insulated. In this dissertation, their work is extended to include a sinusoidally heated top wall.

The nonlinear coupled equations are solved using the Penalty Galerkin Finite Element Method. Stream function and isotherm results are found for various values of the Reynolds number and the Grashof number. The strength of the circulation is seen to increase with increasing Grashof number and to decrease with increasing Reynolds number for both cases of heating. A comparison is made between the stream function

and isotherm results for the two cases.

The results for the rate of heat transfer in terms of the Nusselt number are discussed. Both local and average Nusselt number results are presented and discussed. The average Nusselt number is found using Simpson's 1/3rd rule. The rate of heat transfer is found to be higher at all four walls for the case of cooled side walls than that of linearly heated side walls.

Declaration

The work described in this dissertation was carried out under the supervision of Prof. P. Sibanda, School of Mathematical Sciences, University of KwaZulu-Natal (PMB), from February 2008 to September 2010.

No portion of the work referred to in this dissertation has been submitted in support of an application for another degree or qualification of this or any other university or institution of learning. The dissertation is my original work except where due reference and credit is given.

Signature: .....

Signature: .....

Date: .....

Dedication

To the Lord God Almighty, who made all of this possible.

"The LORD lives!

Praise be to my Rock!

Exalted be God my Savior!" Psalm 18:46

Acknowledgements

I am grateful to my supervisor, Prof. Precious Sibanda for encouraging me in my work and for giving me the space to struggle through concepts and difficulties in my own capacity. I am also grateful to Kanagaratnam Arunakirinathar for giving up his time to meet with me and for his help in the understanding of reduced integration. I am also particularly grateful to Juan Heinrich for his invaluable help in understanding the finite element method. Thank you for making time in your very busy schedule to respond to my emails. I really appreciated your willingness to help.

I am grateful for the financial support that I have received over the course of my masters and am particularly grateful for the funding I received from NRF which enabled me to continue in my studies.

To my parents, thank you for your financial support, not only through this masters process, but throughout high school and my undergraduate degree. Thank you for placing such a high value on my education and for always encouraging me to study

further. Thank you also for your emotional support.

To my husband, I cannot thank you enough. You have been there for me when things were difficult, when I wanted to give up you encouraged me to keep going, when things went well you celebrated with me. I am so lucky to have you in my life.

Chapter 1

Introduction

1.1 History of the problem

Human kind has held a fascination with fluid flow for centuries. From the ebb and flow of the sea and raging rivers, to small ponds and controlled cooling mechanisms, the study, understanding and prediction of fluid flow patterns has a certain attraction to it. In the fifteenth century Leonardo Da Vinci responded to this attraction by observing and recording the phenomenon that we recognize today as a fundamental law of physics; namely the conservation of mass in various flowing rivers. Da Vinci was also one of the first to undertake the task of sketching various flow fields, Anderson [1]. The study of fluid dynamics has changed a lot since Da Vinci's time, yet the fascination has not receded.

Central to the study of modern fluid dynamics are the Navier-Stokes equations. These

equations are so named after Claude-Louis Navier and George Gabriel Stokes (see Tokay [44]). Not only do the Navier-Stokes equations have many applications in the physical world, they are also interesting from a purely mathematical point of view. Although the Navier-Stokes equations have been studied extensively, it has not yet been proven that a general solution of these equations exists, nor if it exists, if the solution is unique (Bresch and Desjardins [10], Chen et al. [14]).

One of the most widely investigated solutions to the Navier-Stokes equations is that of flow within a square cavity. The popularity of such studies is due to the simplicity of the geometry of the problem and the wealth of previous research for the comparison of results, making it easy to use the problem as a prototype for testing and proving new solution techniques. The simplest cavity problem is the lid driven cavity problem. The boundary conditions for such a problem are simple - the lid of the cavity is moved at a constant speed while the other three walls remain stationary. The movement of the fluid in the cavity due to these boundary conditions is known as forced convection because the moving lid is solely responsible for the fluid movement. The lid driven cavity problem is not the only example of forced convection, although it is the most popular. Movement of any of the sides of a cavity results in forced convective flow.

The non-dimensional form of the equations for the forced convection contain a dimensionless variable known as the Reynolds number, Re. The Reynolds number is the ratio of inertia to viscosity (Tritton [46]).

Kawaguti [25] was one of the first to investigate the effect of the Reynolds number

on forced convection in a square cavity. Results were found using finite difference methods for values of the Reynolds number between 0 and 64 for different ratios of lengths of the cavity. An attempt was made to find results for $Re = 128$, but a convergent solution was not found.

By modifying Kawaguti's finite difference method, Burggraf [11] was able to attain stable solutions for forced convection for Reynolds number up to 1000. Streamline results were shown for $Re = 0$, 100 and 400. It was observed that the pattern of the streamlines is only slightly affected by the magnitude of the Reynolds number. However, with increasing Reynolds number, the vortex centre was seen to migrate towards the centre of the cavity.

Heinrich and Marshall [21] used the penalty finite element method to investigate lid driven cavity flow up to a Reynolds number of 400. For low Reynolds number, their results were in excellent agreement with previous results. As the Reynolds number increased however, their results were less accurate in comparison to results from other studies. They suggested refining the finite element mesh close to the boundaries to improve the accuracy of the method.

As mentioned, the lid driven cavity problem is often used as a benchmark problem to test and refine new solution methods. Das and Kanna [17] used previous results of the lid driven cavity problem to test their method, the Alternate Direction Implicit (ADI) scheme as well as to study periodic solutions. They found that the velocity distribution was in good agreement with previous benchmark results and that at

$Re = 10000$ the flow had an oscillating nature.

Another important aspect of the cavity problem is as a prototype for the study of natural convection. In the study of natural convection, the Navier-Stokes equations are coupled with the heat equation to obtain streamline and temperature distributions for various boundary conditions. In contrast to forced convection, in natural or free convection, the movement of the fluid is solely due to temperature differences within the cavity as all walls of the cavity remain stationary. The non-dimensional form of the Navier-Stokes equations for natural convection flow contains two important parameters; the Rayleigh number and the Prandtl number. The Rayleigh number, Ra describes the relationship between buoyancy and viscosity within a fluid. In order for natural convection to occur, there needs to be instability in the fluid. Instability occurs when the Rayleigh number exceeds a critical value which has been found in previous studies to be 1700. Below this value the fluid remains at rest. The Prandtl number Pr is the ratio of diffusivity of momentum to diffusivity of heat (Tritton [46]).

Natural convection has been widely studied over the years. Ostrach [30] gives an excellent overview of early experiments. The first studies of natural convection in a cavity were of an experimental nature. An example of an early experimental study is that of Eckert and Carlson [19]. They made an experimental investigation into the flow and heat transfer of air in an enclosed cavity. The top and bottom plates were heated to different temperatures. Their results showed that, contrary to previous beliefs, it was very unlikely that a core of uniform temperature could exist at large

Rayleigh numbers unless the height to width aspect ratio was very small.

Batchelor [8] was one of the first to investigate a problem of this nature numerically. His motivation was to study a problem that had applications to double glazed windows for the thermal insulation of buildings. Because of this, his focus was on rectangular domains with vertical height much greater than horizontal height. He investigated heat transfer in a cavity with isothermal vertical walls with insulated top and bottom wall. Following on from Batchelor, Poots [34] investigated heat transfer in an air filled cavity with one cooled and one heated side wall. He compared his data with previous experimental data and found similarities in the results. He found that for $Ra = 10^4$, an isothermal core exists in the cavity, which confirmed the findings of Batchelor.

A relatively early study in natural convection was made by De Vahl Davis [18]. A cavity with linearly heated side walls and either linearly heated or adiabatic top and bottom walls was considered. They discovered a development of a boundary layer as the Rayleigh number increased. They also showed that reverse flow is possible near the centre of the cavity at very high Rayleigh numbers. Taylor and Ijam [43] investigated flow within an enclosed cavity using the finite element method. They investigated the effect of varying the Rayleigh and Prandtl numbers when the left side wall was cooled and the right side wall was heated. They investigated the onset of secondary and tertiary flows and these correlated with previous results that were obtained experimentally. They discovered that the existence of secondary flows was

related to the aspect ratio. They also found that the average Nusselt number decreased with increasing aspect ratio. The Nusselt number is the ratio of convective to conductive heat transfer across the boundary.

In a related study, Marshall et al. [27] investigated flows with a heated left side wall and heated right side wall. The top and bottom walls were well insulated. They investigated flow for much lower values of the Prandtl number than Taylor and Ijam [43], but the pattern of the streamlines was very similar for low Rayleigh numbers. They used the finite element method to obtain solutions for the fluid flow and temperature variations for Rayleigh number up to 10^7. They found that their results were in good agreement with previously published results that used the finite difference method. The strength of circulation was seen to increase with an increase in Rayleigh numbers. A large increase in circulation was seen between $Ra = 10^3$ and 10^4, and thereafter the increase followed a power law relationship between the values of Ra and the centre of the vortex.

More recently, Basak et al. [5] investigated the simple case of fluid flow in a cavity with a heated bottom and cooled side walls with the top wall well insulated. They investigated two cases with the bottom wall uniformly and non uniformly heated. The penalty finite element method was used to obtain the results. Streamline patterns show two circulations moving in opposite directions for different values of Prandtl and Rayleigh numbers. They discovered that as the Rayleigh number increased, the strength of the circulations increased.

In a further investigation, Sayithamoorthy et al. [40] studied the effects of linearly heated side walls with a sinusoidally heated bottom wall, while the top wall remained well insulated. Again the penalty finite element method was used. Fluid flow and temperature variations were recorded for various values of the Prandtl number and temperature difference aspect ratio. It was found that for low values of the Prandtl number, many secondary circulations were formed at the bottom of the cavity for all values of the temperature difference aspect ratio. However when the Prandtl number increased above $Pr = 0.7$, only one pair of secondary circulations remained. It was also observed that as the temperature difference aspect ratio increases, the average Nusselt number decreases linearly.

Corcione [16] investigated the effect of the Rayleigh number and the width to height aspect ratio of the cavity on steady laminar natural convection in an air filled cavity. The cavity was heated from below and cooled from above while six different cases of sidewall heating and cooling were investigated using the finite difference approximations and the SIMPLER algorithm (semi-implicit method for pressure linked equations revised). They showed that the heat transfer rate from a cooled or heated boundary increased as the Rayleigh number increases. In the case with insulated side walls, the heat transfer rate from the heated bottom wall or top cooled wall increased as each of the side walls is replaced by a cooled or heated sidewall.

Pesso and Piva [33] investigated the popular case of natural convection in a cavity with one side wall cooled and the other heated while the top and bottom walls are well

insulated. They discovered that the heat transfer rate as measured by the Nusselt number increased with an increase in the Prandtl number. This was particularly true for high Rayleigh numbers.

Sarris et al. [39] investigated fluid flow when the top wall was sinusoidally heated and the other walls were well insulated. Results were found for a wide range of variations in the Rayleigh number. As the Rayleigh number increased, the strength of the circulations was found to increase. The centres of the circulations were seen to move towards the corners of the upper walls with increasing Rayleigh number. The local Nusselt number at the upper wall was also seen to increase with increasing Rayleigh numbers.

Research has also been done into the effect of partial heating of certain walls on natural convection. Aydin and Yang [4] investigated natural convection in a square enclosure with a heat source in the bottom wall while the side walls were cooled. They investigated the effect of the Rayleigh number and the non-dimensional isothermal heat source length on the fluid flow and heat transfer using finite difference approximations. They discovered that increasing the length of the heat source enhanced heat transfer, particularly for high Rayleigh numbers.

Calgani et al. [12] conducted both an experimental and a numerical investigation into the heating of fluid in a square cavity with a heat source in the bottom wall. The numerical investigation was carried out using the finite volume method. The length of the heat source was varied. The two side walls were cooled and the top

wall was kept insulated. They showed that for Rayleigh numbers less than 10^4, the heat transfer was conductive, while at $Ra = 10^5$ the heat transfer was found to be convective. An increase in the length of the heat source produced an increase in heat transfer, particularly at high Rayleigh numbers as was expected.

Bilgen and Yedder [9] studied natural convection with non uniform heating. One sidewall had a varying temperature while the other walls were well insulated. The side wall with varying temperature was divided into two equal parts. Two cases were considered. In the first case, the lower part of the wall was sinusoidally heated while the upper part was sinusoidally cooled and in the second case, the upper part of the wall was heated and the bottom cooled. Results were found for variations of the Rayleigh number and the aspect ratio. They found that a horizontal symmetry occurred for both the streamline and isotherm patterns. They also found that when the lower half was heated, the heat transfer was higher than when the upper half was heated, especially for high Rayleigh numbers.

Cheikh et al. [13] studied natural convection of air in a square cavity using the finite difference method. The cavity was cooled from above and had a heat source in the bottom wall. They investigated the effect of various methods of cooling the side walls. It was found for a cooled top and side wall and heat source at the bottom that the Nusselt number was a maximum. No significant changes in the heat transfer rate were observed for the other thermal boundary conditions studied.

Nithyadevi et al. [29] studied the case where the side walls were partially heated or

partially cooled while the rest of the cavity was well insulated. They used the finite volume method to solve the equations. They studied nine different cases where the position of the heating and cooling sources were moved between the top, bottom and middle of the wall of the cavity. They found that the heat transfer rate was enhanced when there was a cooling source near the top of the cavity. For a combination of a bottom top heating source, the heat transfer rate was found to be high, while for the combination of a top bottom heating source, the heat transfer rate was low.

A third type of convection found in the study of the cavity problem is mixed convection. In mixed convection the movement of fluid is due to a combination of both moving walls and temperature differences within the cavity. Mixed convection is characterised by the Grashof number. The Grashof number, Gr is an indicator of the type of convection to be expected in the fluid. It is the ratio of buoyancy to viscous forces acting on the fluid, Tritton [46].

Torrance et al. [45] investigated the fluid motion with a moving upper wall that is maintained at a different temperature to that of the other walls in the cavity. They held the Reynolds and Prandtl numbers fixed and varied the height to width ratios of the cavity and the Grashof number. They observed that an increase in the aspect ratio led to an increase in secondary circulations in the lower part of the cavity.

Basak et al. [6, 7] in two different papers investigated the effects of mixed convection in a square cavity. Both papers have an insulated moving upper lid. In [7] they looked at cooled side walls with a heated (uniformly and non-uniformly) bottom wall. In

[6] they looked at a uniformly heated bottom wall with linearly heated left side wall. The right side wall was heated either linearly or cooled uniformly. Both papers use the penalty finite element method to solve the resulting equations. Streamlines and temperature contours were found for various variations of the Prandtl, Reynolds and Grashof numbers. Both papers found that the strength of convection increased with increasing Grashof numbers and that lid driven flow was dominant for $Gr = 10^3$. In [7] they found that the effect of natural convection decreased and the effect of forced convection increased with increasing Reynolds number. They also found that the heat transfer rate for the uniformly heated bottom wall was higher than that of the non uniformly heated bottom wall. In [6] they found that the heat transfer rate was larger for the case of one cooled right wall than it was when both walls were linearly heated. This was especially the case for large Grashof numbers.

Prasad and Koseff [36] investigated mixed convection in a lid driven cavity through experimental means where the lower surface was heated and the upper surface cooled. The lid speed and values of the Reynolds and Grashof numbers were varied. They discovered that the heat transfer coefficient was insensitive to increases in Gr/Re^2. Their results indicated that overall heat transfer rate was a very weak function of Gr for the range of Re examined.

Moallemi and Jang [28] investigated flow in a lid driven cavity with the bottom wall heated. They studied the effects of small Prandtl numbers on the flow and heat transfer in a square cavity for various values of the Richardson number. The

Richardson number, Ri is the ratio of potential to kinetic energy and is defined as $Ri = Gr/Re^2$. The temperature and flow fields in the cavity were calculated and presented to illustrate the strong influence of Prandtl number. The local and average Nusselt numbers were also reported for various values of the Reynolds, Prandtl and Grashof numbers.

Oztop and Dagtekin [31] used the finite volume method to investigate three cases of moving walls with adiabatic top and bottom wall and cooled left wall and heated right wall. The three cases included moving the left wall upwards and the right wall downwards, moving the left wall downwards and the right wall upwards and moving both walls upwards. They observed that both the Richardson number and direction of moving walls affect the fluid flow and heat transfer in a cavity. In order to measure the effect of the Richardson number, the Grashof number was fixed at 10^4 and the Reynolds number was varied. They note that for $Ri < 1$ there is a forced convection dominated regime, $Ri > 1$ is the natural convection dominated regime and $Ri = 1$ is the mixed one. For $Ri > 1$, the average Nusselt number was relatively low and for $Ri < 1$ it was relatively higher. When $Ri < 1$, for the cases when the vertical walls move in opposite directions, the heat transfer rate was enhanced regardless of which side moved upwards. When the vertical walls moved upwards in the same direction, the heat transfer rate was reduced compared to the other two cases.

Cheng and Liu [15] investigated four cases of mixed convection in a square cavity. In the first case, the side walls were well insulated while the top moving wall was heated

and the bottom wall cooled. In the second case, the bottom wall was heated and the top wall cooled. In the third and fourth cases, the top and bottom walls were well insulated and one side wall was cooled while the other was heated. In order to vary the Richardson number, the Grashof number was fixed at $Gr = 10^6$ and the Reynolds number was varied. They found that for the first case when the Richardson number was greater than 1 that the heat transfer was mainly through conduction. When the Richardson number was less than 1, forced convection dominated the fluid flow as was found by Oztop and Dagtekin [31]. In contrast to the findings of Oztop and Dagtekin, in the second case, when the Richardson number was greater than 1, the lower half of the cavity showed natural convection while the upper part was dominated by forced convection. This was due to the difference in heating of the cavities between the two studies. When the Richardson number was less than 1, the fluid flow was similar to that of case 1. For the third case when the Richardson number was greater than 1, heat transfer was shown to be by conduction near the side walls and by convection in the centre. Again when the Richardson number was less than one, the fluid flow was similar to that of cases 1 and 2. For the fourth case, a large portion of the cavity was dominated by natural convection for all values of the Richardson number. The thermal boundary conditions for the fourth case were identical to the study of Oztop and Dagtekin [31], but the effect of the Richardson number of fluid flow was seen to be different. This is due to the fact that Cheng and Liu [15] investigated mixed convection with a moving lid while Oztop and Dagtekin

[31] investigated mixed convection with moving side walls.

Wong [48] investigated mixed convection in a square cavity. The left wall was maintained at a constant velocity. The other walls were kept stationary. The top and bottom walls were insulated and the left moving wall was heated while the right side wall was cooled. A numerical solution was found using the consistent splitting scheme and the finite element method. Wong fixed the Reynolds number at 100 and varied the Grashof number to measure the effects of the Richardson number. The effect of the Richardson number on the fluid flow was investigated. When the Richardson number was 0.001, the flow was found to be strongly influenced by forced convection. At $Ri = 1$, mixed convection is found to occur. At $Ri = 100$, the fluid flow is mainly dominated by natural convection. These findings are similar to those of Oztop and Dagtekin [31] even though only one side wall was moving in this case.

Prasad and Das [35] investigated mixed convection in a rectangular cavity where all four walls were moved at a constant velocity and the top wall was heated while all three other walls were cooled. The Reynolds number was kept stationary at 100 and the Grashof number was varied between positive and negative values. The aspect ratio (ratio of height to width of the cavity) was also varied. The finite volume SIMPLE (semi-implicit method for pressure linked equations) algorithm was used to solve the resulting equations. They found that as the negative Grashof number increased, heat transfer was dominated by convection. For the aspect ratio of 2, the flow was seen to undergo a Hopf Bifurcation at $Ra = -10^5$.

Sivakumar et al. [42] investigated mixed convection in a lid driven cavity with a cooled right wall and a heat source in the left wall. The remaining portion of the left wall as well as the top and bottom walls were well insulated. Three different lengths of the heat source were examined. The finite volume method was used to solve the resulting equations. Streamline patterns were observed and it was found that for low values of the Richardson number, reducing the heating portion length had no effect on the fluid flow. However, on increasing the Richardson number it was seen that the flow depended heavily on the length of the heat source. It was also found that reducing the length of the heated portion of the left wall resulted in a better heat transfer rate.

1.2 Applications of the problem

The movement of fluids has many uses in the industrial and natural worlds because moving fluids transport heat (Tritton [46]).

Natural convection is of great importance, for example, in the cooling of electronic equipment. Electronic equipment generates heat when in use and it is essential to cool down the equipment for reliable functioning. Natural convection is a simple and cost effective method of cooling equipment (Aydin and Yang [4]). Another application of vital importance is the cooling of nuclear reactors. The nuclear reactor core is surrounded by a gas filled cavity and natural convection provides an effective

means of cooling this cavity (De Vahl Davis [18]). The study of natural convection is also important in the design of buildings and rooms in order to provide adequate ventilation and make them energy efficient (Basak et al. [5]).

Other applications of natural convection can be found in lubrication technologies, drying technologies (Oztop and Dagtekin [31]), double glazed windows (De Vahl Davis [18]), solar energy collection and fire control (Basak et al. [7]). Mixed convection flow has further applications in mass and heat transfer, for example, in solar ponds, in the dynamics of lakes, thermal-hydraulics of nuclear reactors and in food processing (Basak et al [6]).

1.3 Solution methods

The equations that govern the flow of fluid and convection in a cavity are nonlinear with no known analytical solutions. It is therefore necessary to solve the equations using numerical methods. Although many methods have been used to solve these equations, the most common methods in the literature used to solve natural or mixed convection in a square cavity are various forms of the finite difference method, the finite volume method and the finite element method.

1.3.1 The Finite Element Method

The finite element method is an increasingly popular solution method. Researchers such as Basak et. al. [5, 6, 7] and Sayithamoorty [40], Heinrich and Marshall [21] and Taylor and Ijam [43] use the finite element method exclusively in their research.

The basic idea of the finite element method is to divide the geometry of the problem into subdomains, establish an equation for each element and then assemble these together to solve the problem. The idea of dividing a problem into subdomains is not a new concept. Ancient mathematicians used such ideas to estimate the value of π. They realised that in order to estimate the circumference of a circle, they could calculate the perimeter of a polygon inscribed in the circle. In fact they managed to estimate π to an accuracy of almost forty significant digits simply by using this method (Reddy [38]).

The development of the finite element method can be traced back to the work of Hrenikoff and Courant in the early 1940s. However, the actual term finite element only came into being in 1960 and was first used by Clough (see Reddy [38]). The finite element method really took off in the late 1950s. In 1965, NASA requested that finite element software called Nastran be developed ([47]). Today the finite element method is used to solve many problems in the industrial world.

The finite element method can be divided into four basic steps.

- Firstly the domain of the problem is divided into n finite elements. The elements

are connected to one another at nodes. The most commonly shaped elements are triangular or rectangular.

- Secondly, an equation is formulated for each element. The solution u is represented as a linear combination of approximation functions.

- Thirdly, the element equations are assembled together to obtain equations for the whole problem.

- And fourthly boundary conditions are imposed on the equations (Gresho and Sani [20], Reddy [38] and Zienkiewicz [49]).

There are a number of different versions of the finite element method which differ in the way in which the weight and approximation functions are defined. The method of Weighted Residuals uses what is known as the Residual of the approximation. For example if one wishes to solve a general equation

$$A(u) = f \in \Omega,$$

where A can be a linear or nonlinear operator, then the residual of the approximation is

$$R = A(u_N) - f,$$

where u_N is the approximation of the variable u. In general the residual will be nonzero. In the method of weighted residuals the approximation functions are determined by requiring that the weighted integral of the residual is equal to 0. The

weighted integral is the integral of the residual multiplied by a weight function. It is in choosing the weight and approximation functions that different methods arise. In the Petrov-Galerkin method, the weight function and the approximation functions are chosen in such a way that the two are not equal to one another. In the Galerkin method, the weight function is chosen to be equal to the approximation function. Another commonly used finite element method is the least squares method. In the least squares method, the approximation functions are determined by finding the minimum of the integral of the square of the residual. The Galerkin method is one of the most popular methods due to its simplicity and the fact that one only has to chose one function to be the weight and the approximation functions. Because of this popularity, the terms "method of weighted residuals" and the "Galerkin method" are often used interchangeably (Reddy, [38]).

1.3.2 The Finite Difference and Finite Volume Methods

The finite difference method was very popular among early researchers investigating the flow and convection in a square cavity. For example, the finite difference method was used by both Kawaguti [25] and Burggraf [11] in some of the very first investigations of flow within a cavity. Although the finite difference method is still used today, its popularity has declined with the development of the finite volume and finite element methods, both of which provide certain advantages over the finite difference method. The finite volume method is a very popular method today and has been

used by researchers such as Oztop and Dagtekin [31], Sivakumar et. al. [42] and Prasad and Koseff [36] to solve problems of convection in a square cavity.

The finite difference and finite volume methods have many similarities. In fact "the finite volume method can often be interpreted directly as a finite difference approximation to the differential equation" (Leveque [26]). As in the finite element method, the domain is divided into intervals. In the finite volume method, these intervals are known as volumes.

In the finite difference method, the derivatives of the governing equation are replaced by linear combinations of function values (Iserles [24]). The differential equation is thus replaced with algebraic equations which can then be solved to find an approximate solution (Ascher [3]). The finite difference method uses a pointwise approximation at the grid points and is well known for its simplicity.

In contrast to the finite difference method, the finite volume method is based on the integral form of the equation rather than the differential equation. This has its advantages in that the integral form is "closer to the physics than the partial differential equation," (Leveque [26]). Another difference between the finite volume and finite difference methods is that the finite volume method does not use pointwise approximation. Instead the average of the integral over each grid cell is approximated (Leveque [26]). Finite volume methods are particularly effective at solving problems with discontinuities.

1.3.3 Advantages of the Finite Element Method

Supporters of the finite element are plentiful. In fact Reddy [38] describes the finite element method as "the most powerful numerical method ever devised for the analysis of engineering problems."

The advantages of the finite element method are numerous:

- The major advantage of the finite element method is its effectiveness in handling complex geometries. Because each element in the finite element method is unique and the elements do not need to be orthogonal, the elements can be manipulated to fit even the most complex of geometries by combining triangular and rectangular elements of varying sizes. Although finite difference and finite volume methods have come up with ways to tackle complex geometries in recent history, finite elements are the simplest and most effective methods for dealing with complex geometries (Gresho and Sani [20], Iserles [24] and Huebner et al. [22]).

- Because the element equations are evaluated individually, finite element methods have the advantage of being able to solve problems involving different materials within a domain (Akin, [2]).

- The finite element method is more efficient at dealing with Neumann boundary conditions than the finite difference and finite volume methods. Both the finite

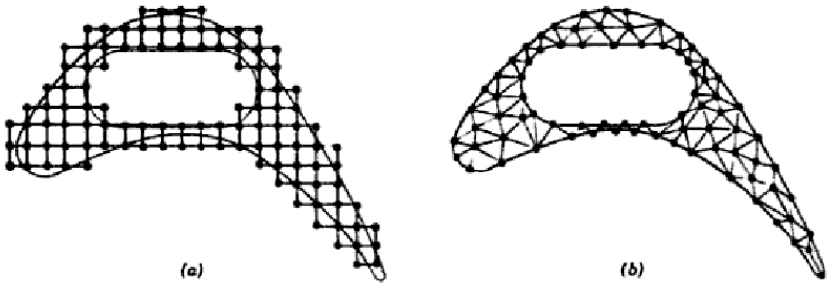

Figure 1.1: Comparison of a finite difference (a) and finite element (b) mesh for a complex geometry. Source: Huebner et al. [22]

difference and finite volume methods handle Dirichlet boundary conditions easily as the values are simply inserted into the solution, but in order to implement derivative boundary conditions, the equations need to be modified (Saleh [41]).

- Another advantage of the finite element method, is that the matrices are created for each element first, and these are then assembled together to form the global equations before the problem is solved. In the finite volume and finite difference methods, the process of setting up the equations and solving the equations is combined. Because this process is decoupled in the finite element method, the addition of new element types is relatively easy to achieve. However, adding new cell types in the finite volume method can be quite difficult and the finite volume method can exhibit problems if it has multiple cell types (Saleh [41]).

- The finite element method has an advantage over the finite volume method

in that if the original differential operator is symmetric so too are the finite element discretisations of the operator, but this is not always the case for the finite volume method on non rectangular grids (Gresho and Sani [20]).

- Another advantage over finite volume methods is that the Galerkin finite element method is always more accurate than the corresponding finite volume method for elliptic problems (Gresho and Sani [20]).

In general both the finite element and finite volume methods are efficient at solving the Navier-Stokes and energy equations in a square cavity and each method has its own advantages. The use of either method is simply a matter of preference. Due to the above advantages of the finite element method, it is the method of choice in this investigation.

1.4 Current Investigation

In this study, mixed convection in a two dimensional square cavity will be investigated. Much work has been done on natural convection in a cavity, the most common cases being to heat one of the side walls and cool another, or to heat the bottom wall. Not much work has been done on sinusoidal heating of walls and even less has been done on a combination of linear and sinusoidal heating. Sathiyamoorthy et al. [40] is one of the few to investigate this combination.

The intention of this investigation is to combine linear and sinusoidal heating of

different walls of the cavity with a moving lid to provide mixed convection. This is an extension of work done by Basak et al. [6] where linear heating of the side walls is combined with a moving lid. Specifically, the adiabatic top wall of Basak et al. [6] will be replaced by a sinusoidally heated top wall in this investigation. All other boundary conditions will remain the same. The second aim of this investigation is to extend the work done by Basak et al. [7] where cooled side walls are investigated instead of linearly heated walls. Again, comparisons will then be made with the results obtained by Basak et al. [7] and further comparisons will be made between the two cases of side wall heating.

The Penalty Finite Element Method will be used to solve the flow equations. The advantage of this method over the ordinary Finite Element Method is that it eliminates pressure as a variable.

The dissertation is structured as follows:

- In Chapter 2 we formulate the problem mathematically. This includes looking at the finite element formulation using the Penalty Galerkin Method, as well as the stream function and Nusselt Number formulations.

- In Chapter 3 we present the results found for the two cases in terms of streamline and isotherm contours and local and average Nusselt numbers. Comparisons are made between the two cases and with previous results.

- Finally, in Chapter 4 we present our conclusions.

Chapter 2

Problem Formulation and Numerical Method

2.1 Problem Formulation

A two-dimensional square cavity of unit length is considered for the current investigation, the geometry of which is shown in Figure 2.1. Two cases are considered. In case 1, the cavity is heated at a constant rate from the bottom and heated linearly at the side walls. The lid of the cavity is heated sinusoidally while moving at a constant speed from left to right. In case 2, the cavity is again heated at a constant rate from the bottom and heated sinusoidally from the top with a moving lid. However, in this case the side walls are uniformly cooled.

The viscous incompressible flow and the temperature distribution in the cavity are

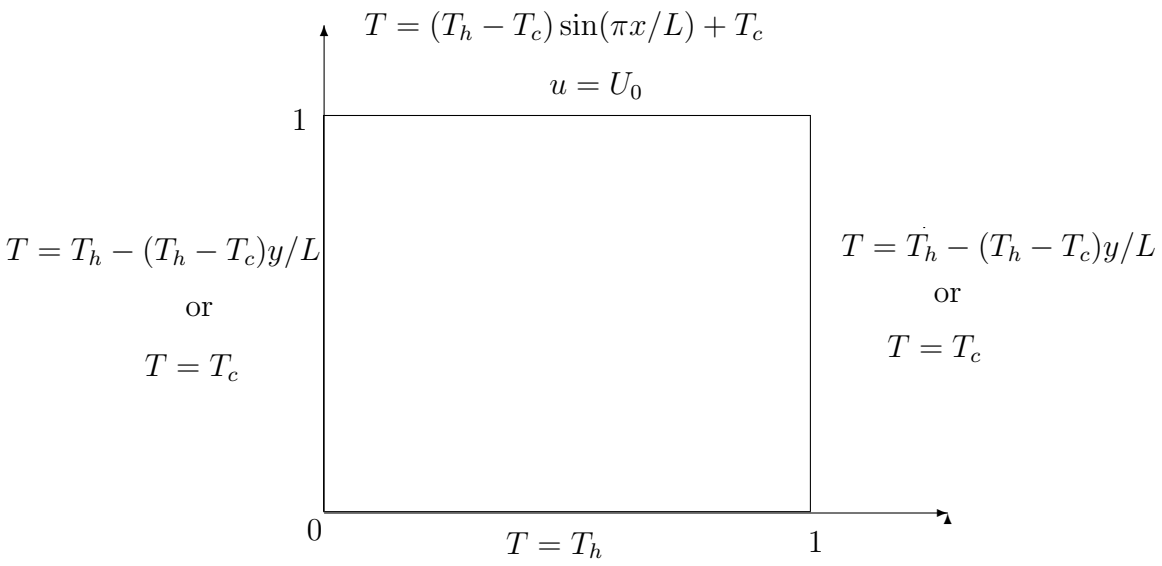

Figure 2.1: Schematic sketch of the cavity problem. The two different cases of thermal boundary conditions are investigated separately.

governed by the Navier-Stokes equations and the energy equation respectively. In this investigation, density is treated in line with the Boussinesq approximation. In the Boussinesq approximation, density is assumed to be constant, except in the gravity term where the density ρ is multiplied by the acceleration due to gravity, g (Pepper and Heinrich [32]).

The equations to be solved are as follows (see for example, Basak et al. [7]):

$$\frac{\partial u}{\partial x} + \frac{\partial v}{\partial y} = 0, \tag{2.1}$$

$$u\frac{\partial u}{\partial x} + v\frac{\partial u}{\partial y} = -\frac{1}{\rho}\frac{\partial p}{\partial x} + \nu\left(\frac{\partial^2 u}{\partial x^2} + \frac{\partial^2 u}{\partial y^2}\right), \tag{2.2}$$

$$u\frac{\partial v}{\partial x} + v\frac{\partial v}{\partial y} = -\frac{1}{\rho}\frac{\partial p}{\partial y} + \nu\left(\frac{\partial^2 v}{\partial x^2} + \frac{\partial^2 v}{\partial y^2}\right) + g\beta(T_h - T_c), \tag{2.3}$$

$$u\frac{\partial T}{\partial x} + v\frac{\partial T}{\partial y} = \alpha\ \left(\frac{\partial^2 T}{\partial x^2} + \frac{\partial^2 T}{\partial y^2}\right), \tag{2.4}$$

subject to the boundary conditions (see Fig 2.1)

$$u = v = 0,\ T = T_h - (T_h - T_c)\frac{y}{L}\ or\ T = T_c \quad \text{at} \quad x = 0 \quad \text{and} \quad x = 1, \tag{2.5}$$

$$u = v = 0,\ T = T_h \quad \text{at} \quad y = 0 \tag{2.6}$$

$$u = U_0,\ v = 0,\ T = (T_h - Tc)\sin(\pi\frac{x}{L}) + T_c \quad \text{at} \quad y = 1, \tag{2.7}$$

where u and v are the velocity components in the x and y directions respectively, T is the fluid temperature, ν is the kinematic viscosity, α is the thermal diffusivity, β is the coefficient of thermal expansion, g is the acceleration due to gravity, ρ is the mass density, L is length of the cavity, U_0 is the velocity of the upper wall, T_h is the hottest temperature attained along the bottom wall and the middle of the top wall

and T_c is the coolest temperature attained at the top corners in case 1 and attained along the side walls in case 2.

Using the following change of variables (as used by Basak et al. [7]),

$$\begin{aligned} X &= \frac{x}{L}, \quad Y = \frac{y}{L}, \quad U = \frac{u}{U_0}, \quad V = \frac{v}{U_0}, \\ \theta &= \frac{T - T_c}{T_h - T_c}, \quad P = \frac{p}{\rho U_0^2}, \quad Pr = \frac{\nu}{\alpha}, \\ Re &= \frac{U_0 L}{\nu}, \quad Gr = \frac{g\beta(T_h - T_c)L^3}{\nu^2}, \end{aligned}$$

where θ is the dimensionless temperature, Pr is the Prandtl number, Re is the Reynolds number, and Gr is the Grashof number, we obtain the following dimensionless equations:

$$\frac{\partial U}{\partial X} + \frac{\partial V}{\partial Y} = 0, \tag{2.8}$$

$$U\frac{\partial U}{\partial X} + V\frac{\partial U}{\partial Y} = -\frac{\partial P}{\partial X} + \frac{1}{Re}\left(\frac{\partial^2 U}{\partial X^2} + \frac{\partial^2 U}{\partial Y^2}\right), \tag{2.9}$$

$$U\frac{\partial V}{\partial X} + V\frac{\partial V}{\partial Y} = -\frac{\partial P}{\partial Y} + \frac{1}{Re}\left(\frac{\partial^2 V}{\partial X^2} + \frac{\partial^2 V}{\partial Y^2}\right) + \frac{Gr}{Re^2}\theta, \tag{2.10}$$

$$U\frac{\partial \theta}{\partial X} + V\frac{\partial \theta}{\partial Y} = \frac{1}{RePr}\left(\frac{\partial^2 \theta}{\partial X^2} + \frac{\partial^2 \theta}{\partial Y^2}\right). \tag{2.11}$$

The dimensionless boundary conditions are (see Figure 2.2):

$$U = V = 0, \ \theta = 1 - Y \text{ or } 0 \quad \text{at} \quad X = 0 \quad \text{and} \quad X = 1, \tag{2.12}$$

$$U = V = 0, \ \theta = 1 \quad \text{at} \quad Y = 0 \tag{2.13}$$

$$U = 1, \ V = 0, \ \theta = \sin(\pi X) \quad \text{at} \quad Y = 1. \tag{2.14}$$

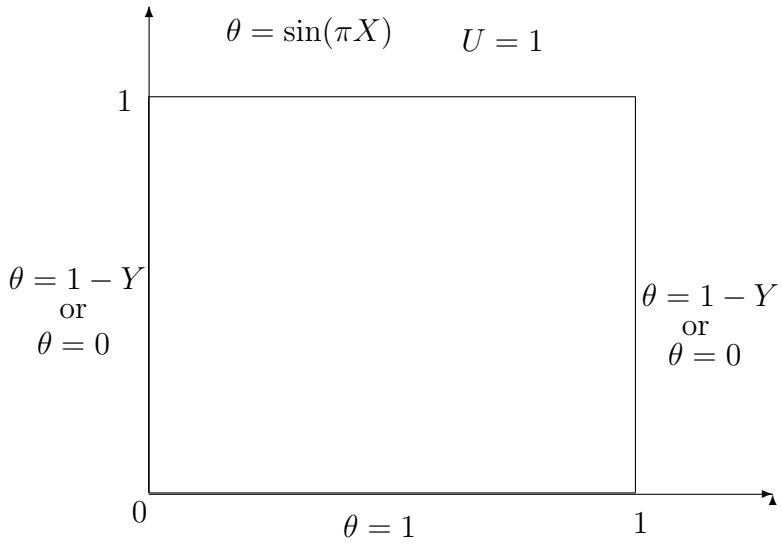

Figure 2.2: Schematic sketch of the cavity problem with dimensionless boundary conditions. The different thermal boundary conditions on the sides of the cavity are investigated separately.

2.2 Numerical Solution

The equations are solved using the Penalty Galerkin Finite Element method. When the Navier-Stokes equations are expressed in terms of the stream function and vorticity, the continuity equation is satisfied through the stream function, which is extremely useful. However, the use of the stream function and vorticity form of the Navier-Stokes equations results in difficulties in the imposition of certain boundary conditions, such as stress boundary conditions. It is simpler to impose the boundary conditions if the equations are kept in the velocity-pressure form. When using the penalty function form of the finite element method, the velocity-pressure form of the equations is used, thus ensuring easy imposition of boundary conditions, but the continuity equation is still satisfied and pressure is also eliminated as a dependent variable (Marshall et al. [27]).

2.2.1 Penalty Galerkin Finite Element Method

We start by introducing a test or weight function ϕ_i (where ϕ_i is in the set of piecewise, once differentiable functions) and multiply equations (2.9) - (2.11) by the test function to obtain the weak forms of the equations:

$$\int \phi_i \left[U\frac{\partial U}{\partial X} + V\frac{\partial U}{\partial Y} + \frac{\partial P}{\partial X} - \frac{1}{Re}\left(\frac{\partial^2 U}{\partial X^2} + \frac{\partial^2 U}{\partial Y^2}\right)\right] \partial\Omega = 0, \tag{2.15}$$

$$\int \phi_i \left[U\frac{\partial V}{\partial X} + V\frac{\partial V}{\partial Y} + \frac{\partial P}{\partial Y} - \frac{1}{Re}\left(\frac{\partial^2 V}{\partial X^2} + \frac{\partial^2 V}{\partial Y^2}\right) + \frac{Gr}{Re^2}\theta\right] \partial\Omega = 0, \tag{2.16}$$

$$\int \phi_i \left[U\frac{\partial \theta}{\partial X} + V\frac{\partial \theta}{\partial Y} - \frac{1}{RePr}\left(\frac{\partial^2 \theta}{\partial X^2} + \frac{\partial^2 \theta}{\partial Y^2}\right)\right] \partial\Omega = 0. \tag{2.17}$$

For convenience, equations (2.15) - (2.17) can be written in a divergence form (see Gresho and Sani [20]):

$$\int \phi_i \left(U\frac{\partial U}{\partial X} + V\frac{\partial U}{\partial Y}\right) = \phi_i \nabla \cdot \tau_x, \tag{2.18}$$

$$\int \phi_i \left(U\frac{\partial V}{\partial X} + V\frac{\partial V}{\partial Y}\right) = \phi_i \nabla \cdot \tau_y, \tag{2.19}$$

$$\int \phi_i \left(U\frac{\partial \theta}{\partial X} + V\frac{\partial \theta}{\partial Y}\right) = \phi_i \nabla \cdot \tau_t, \tag{2.20}$$

where

$$\tau_x = e_x \left(\frac{1}{Re}\frac{\partial U}{\partial X} - P\right) + e_y \left(\frac{1}{Re}\frac{\partial U}{\partial Y}\right), \tag{2.21}$$

$$\tau_y = e_x \left(\frac{1}{Re}\frac{\partial V}{\partial X}\right) + e_y \left(\frac{1}{Re}\frac{\partial V}{\partial Y} - P\right), \tag{2.22}$$

$$\tau_t = e_x \left(\frac{1}{RePr}\frac{\partial \theta}{\partial X}\right) + e_y \left(\frac{1}{RePr}\frac{\partial \theta}{\partial Y}\right), \tag{2.23}$$

where e_x and e_y are the cartesian base vectors for x and for y respectively.

Writing the equations in this divergence form now makes it easy to integrate by parts using the divergence theorem. The process is illustrated for the x momentum equation

as follows:

$$\int \phi_i \left(U\frac{\partial U}{\partial X} + V\frac{\partial U}{\partial Y} \right) = \int \phi_i \nabla \cdot \tau_x = \int \nabla \cdot (\phi_i \tau_x) - \int \nabla \phi_i \cdot \tau_x$$
$$= \int_\Gamma \phi_i \mathbf{n} \cdot \tau_x - \int \nabla \phi_i \cdot \tau_x, \quad (2.24)$$

which we rearrange to get

$$\int \left[\phi_i \left(U\frac{\partial U}{\partial X} + V\frac{\partial U}{\partial Y} \right) + \nabla \phi_i \cdot \tau_x \right] = \int_\Gamma \phi_i \mathbf{n} \cdot \tau_x. \quad (2.25)$$

Expanding gives

$$\int \phi_i \left(U\frac{\partial U}{\partial X} + V\frac{\partial U}{\partial Y} \right) + \frac{1}{Re}\frac{\partial \phi_i}{\partial X}\frac{\partial U}{\partial X} - P\frac{\partial \phi_i}{\partial X} + \frac{1}{Re}\frac{\partial \phi_i}{\partial Y}\frac{\partial U}{\partial Y}$$
$$= \int_\Gamma \phi_i \left[n_x \left(\frac{1}{Re}\frac{\partial U}{\partial X} - P \right) + n_y \left(\frac{1}{Re}\frac{\partial U}{\partial Y} \right) \right] \quad (2.26)$$

Similarly, the y momentum and energy equations, after using the same procedure become

$$\int \phi_i \left(U\frac{\partial V}{\partial X} + V\frac{\partial V}{\partial Y} \right) - \frac{Gr}{Re^2}\theta + \frac{1}{Re}\frac{\partial \phi_i}{\partial X}\frac{\partial V}{\partial X} - P\frac{\partial \phi_i}{\partial Y} + \frac{1}{Re}\frac{\partial \phi_i}{\partial Y}\frac{\partial V}{\partial Y} =$$
$$\int_\Gamma \phi_i \left[n_x \left(\frac{1}{Re}\frac{\partial V}{\partial X} \right) + n_y \left(\frac{1}{Re}\frac{\partial V}{\partial Y} - P \right) \right], \quad (2.27)$$

$$\int \phi_i \left(U\frac{\partial \theta}{\partial X} + V\frac{\partial \theta}{\partial Y} \right) + \frac{1}{RePr}\left(\frac{\partial \phi_i}{\partial X}\frac{\partial \theta}{\partial X} + \frac{\partial \phi_i}{\partial Y}\frac{\partial \theta}{\partial Y} \right) =$$
$$\int_\Gamma \phi_i \left[n_x \frac{1}{RePr}\frac{\partial \theta}{\partial X} + n_y \frac{1}{RePr}\frac{\partial \theta}{\partial Y} \right]. \quad (2.28)$$

We let

$$\int_\Gamma \phi_i \left[n_x \left(\frac{1}{Re} \frac{\partial U}{\partial X} - P \right) + n_y \left(\frac{1}{Re} \frac{\partial U}{\partial Y} \right) \right] = F_x, \tag{2.29}$$

$$\int_\Gamma \phi_i \left[n_x \left(\frac{1}{Re} \frac{\partial V}{\partial X} \right) + n_y \left(\frac{1}{Re} \frac{\partial V}{\partial Y} - P \right) \right] = F_y, \tag{2.30}$$

$$\int_\Gamma \phi_i \left[n_x \frac{1}{RePr} \frac{\partial \theta}{\partial X} + n_y \frac{1}{RePr} \frac{\partial \theta}{\partial Y} \right] = F_\theta. \tag{2.31}$$

These are known as the natural boundary conditions, but for simplicity we let F_x, F_y and F_θ equal 0 (see Gresho and Sani [20]).

The continuity equation in its weighted form becomes

$$\int_\Omega \psi_i \left(\frac{\partial U}{\partial X} + \frac{\partial V}{\partial Y} \right) d\Omega = 0. \tag{2.32}$$

The Penalty Method supposes that we replace this with

$$\int_\Omega \psi_i \left(\frac{\partial U}{\partial X} + \frac{\partial V}{\partial Y} \right) d\Omega = -\epsilon P, \tag{2.33}$$

where ϵ is an arbitrarily small number.

Rearranging these equations we find

$$P = -\lambda \nabla \cdot \mathbf{u}$$

where λ is known as the penalty parameter. Clearly,

$$\frac{\partial U}{\partial X} + \frac{\partial V}{\partial Y} \to 0$$

as $\varepsilon \to 0$ or $\lambda \to \infty$.

We now obtain the penalized momentum equations as:

$$\int \phi_i \left(U\frac{\partial U}{\partial X} + V\frac{\partial U}{\partial Y} \right) + \frac{1}{Re}\frac{\partial \phi_i}{\partial X}\frac{\partial U}{\partial X} + \lambda \left[U\frac{\partial}{\partial X}\left(\frac{\partial \phi_i}{\partial X}\right) + V\frac{\partial}{\partial X}\left(\frac{\partial \phi_i}{\partial Y}\right)\right] + \frac{1}{Re}\frac{\partial \phi_i}{\partial Y}\frac{\partial U}{\partial Y} = 0, \quad (2.34)$$

$$\int \phi_i \left(U\frac{\partial V}{\partial X} + V\frac{\partial V}{\partial Y} \right) - \frac{Gr}{Re^2}\theta + \frac{1}{Re}\frac{\partial \phi_i}{\partial X}\frac{\partial V}{\partial X} + \lambda \left[U\frac{\partial}{\partial Y}\left(\frac{\partial \phi_i}{\partial X}\right) + V\frac{\partial}{\partial Y}\left(\frac{\partial \phi_i}{\partial Y}\right)\right] + \frac{1}{Re}\frac{\partial \phi_i}{\partial Y}\frac{\partial V}{\partial Y} = 0. \quad (2.35)$$

2.2.2 Finite Element formulation

We now set out to find the finite element approximate solution of equations (2.28), (2.34) and (2.35). We discretise the domain into four hundred rectangular elements with a total of four hundred and forty four nodes. In principle, more elements may be used to ensure even greater accuracy of results, but this greatly increases the computation time. Initially one hundred elements were used, but although the computation of such a formulation was efficient, the accuracy of the solutions was impaired. Four hundred elements were found to give sufficient accuracy without impairing the efficiency of the solution method.

There are three hundred and sixty one nodes which are not on a Dirichlet boundary. Associated with each node in the domain is a basis function, ϕ_j. The same functions (ϕ_i) will be chosen as test and basis functions. These basis functions are chosen

to be linear Lagrange elements (see Reddy [38]). We now expand U, V and θ as linear combinations of the basis functions over the non-Dirichlet boundary nodes and interpolate the Dirichlet boundary conditions on u, v and θ.

We set

$$U = \sum_{j=1}^{361} U_j \phi_j, \tag{2.36}$$

$$V = \sum_{j=1}^{361} V_j \phi_j, \tag{2.37}$$

$$\theta = \sum_{j=1}^{361} \theta_j \phi_j, \tag{2.38}$$

where U_j, V_j and θ_j are the nodal values of U, V and θ at the j-th node respectively. By substituting these expression for U, V and θ into equations (2.28), (2.34) and (2.35), we obtain (after manipulation and simplification):

$$\begin{aligned}\sum_{j=1}^{361} U_j \int_\Omega \left[\left(\sum_{k=1}^{361} U_k \phi_k \right) \frac{\partial \phi_j}{\partial X} + \left(\sum_{k=1}^{361} V_k \phi_k \right) \frac{\partial \phi_j}{\partial Y} \right] \phi_i dX dY \\ + \lambda \left[\sum_{j=1}^{361} U_j \int_\Omega \frac{\partial \phi_i}{\partial X} \frac{\partial \phi_j}{\partial X} dX dY + \sum_{j=1}^{361} V_j \int_\Omega \frac{\partial \phi_i}{\partial X} \frac{\partial \phi_j}{\partial Y} dX dY \right] \\ + \frac{1}{Re} \sum_{j=1}^{361} U_j \int_\Omega \left[\frac{\partial \phi_i}{\partial X} \frac{\partial \phi_j}{\partial X} + \frac{\partial \phi_i}{\partial Y} \frac{\partial \phi_j}{\partial Y} \right] dX dY = 0, \end{aligned} \tag{2.39}$$

$$\sum_{j=1}^{361} V_j \int_\Omega \left[\left(\sum_{k=1}^{361} U_k \phi_k \right) \frac{\partial \phi_j}{\partial X} + \left(\sum_{k=1}^{361} V_k \phi_k \right) \frac{\partial \phi_j}{\partial Y} \right] \phi_i dX dY$$
$$+ \lambda \left[\sum_{j=1}^{361} U_j \int_\Omega \frac{\partial \phi_i}{\partial Y} \frac{\partial \phi_j}{\partial X} dX dY + \sum_{j=1}^{361} V_j \int_\Omega \frac{\partial \phi_i}{\partial Y} \frac{\partial \phi_j}{\partial Y} dX dY \right]$$
$$+ \frac{1}{Re} \sum_{j=1}^{361} V_j \int_\Omega \left[\frac{\partial \phi_i}{\partial X} \frac{\partial \phi_j}{\partial X} + \frac{\partial \phi_i}{\partial Y} \frac{\partial \phi_j}{\partial Y} \right] dX dY - \frac{Gr}{Re^2} \int_\Omega \left(\sum_{j=1}^{361} \theta_j \phi_j \right) \phi_i dX dY = 0, \tag{2.40}$$

$$\sum_{j=1}^{361} \theta_j \int_\Omega \left[\left(\sum_{k=1}^{361} U_k \phi_k \right) \frac{\partial \phi_j}{\partial X} + \left(\sum_{k=1}^{361} V_k \phi_k \right) \frac{\partial \phi_j}{\partial Y} \right] \phi_i dX dY$$
$$+ \frac{1}{RePr} \sum_{j=1}^{361} \theta_j \int_\Omega \left[\frac{\partial \phi_i}{\partial X} \frac{\partial \phi_j}{\partial X} + \frac{\partial \phi_i}{\partial Y} \frac{\partial \phi_j}{\partial Y} \right] dX dY. \tag{2.41}$$

We can now represent the equations in matrix form:

$$\begin{bmatrix} N(\mathbf{u}) + \lambda K_x + \frac{1}{Re} K & \lambda K_{xy} & 0 \\ \lambda K_{yx} & N(\mathbf{u}) + \lambda K_y + \frac{1}{Re} K & \frac{Gr}{Re^2} M \\ 0 & 0 & N(\mathbf{u}) + \frac{1}{RePr} K \end{bmatrix} \begin{bmatrix} U \\ V \\ \theta \end{bmatrix} = \begin{bmatrix} f_1 \\ f_2 \\ f_3 \end{bmatrix}$$

where

$$N(\mathbf{u}) = \int_\Omega \left[\left(\sum_{k=1}^{361} U_k \phi_k \right) \frac{\partial \phi_j}{\partial X} + \left(\sum_{k=1}^{361} V_k \phi_k \right) \frac{\partial \phi_j}{\partial Y} \right] \phi_i \, dX dY, \tag{2.42}$$

$$K_x = \int_\Omega \frac{\partial \phi_i}{\partial X} \frac{\partial \phi_j}{\partial X} dX dY, \qquad K_y = \int_\Omega \frac{\partial \phi_i}{\partial Y} \frac{\partial \phi_j}{\partial Y} dX dY, \tag{2.43}$$

$$K_{xy} = \int_\Omega \frac{\partial \phi_i}{\partial X} \frac{\partial \phi_j}{\partial Y} dX dY, \qquad K_{yx} = \int_\Omega \frac{\partial \phi_i}{\partial Y} \frac{\partial \phi_j}{\partial X} dX dY, \tag{2.44}$$

$$K = K_x + K_y \qquad M = \int_\Omega \phi_i \phi_j dX dY, \tag{2.45}$$

and f_1, f_2 and f_3 approximate the values of U, V and θ respectively on the Dirchlet boundary.

Each of these matrices is evaluated for each element individually and then assembled into a global coefficient matrix. Gaussian interpolation is then used to evaluate the integrals.

We now have a system of nonlinear equations which we can write in the form

$$(\mathbf{K_1} + \lambda \mathbf{K_2})\mathbf{a} = \mathbf{F}; \tag{2.46}$$

where $\mathbf{K_1}$ contains the non penalized section of the matrix, $\mathbf{K_2}$ contains the penalized section of the matrix, $\mathbf{a}$ and $\mathbf{F}$ are column vectors given by $\mathbf{a} = [U \ V \ \theta]^T$ and $\mathbf{F} = [f_1 \ f_2 \ f_3]^T$.

There are however some difficulties in solving these equations accurately. The first difficulty is in choosing the most appropriate value of λ. If λ is too small, the incompressibility constraint will not be satisfied. In this calculation, λ is chosen as 10^7 the value used by Reddy [38].

The second problem is found in the construction of the matrices $\mathbf{K_1}$ and $\mathbf{K_2}$. The difficulty arises when λ is chosen as a large value (as in this case), this causes the impact of $\mathbf{K_1}$ to be negligible in comparison to $\lambda \mathbf{K_2}$. We therefore obtain

$$\mathbf{K_2 a} = \frac{\mathbf{F}}{\lambda}. \tag{2.47}$$

As $\lambda \to \infty$, we obtain $\mathbf{K_2 a} \to \mathbf{0}$. Using Gaussian interpolation to find $\mathbf{K_2}$ produces a nonsingular matrix and therefore the results obtained are trivial. In order for a nontrivial solution to be found, $\mathbf{K_2}$ must be singular (Reddy [38]). This is achieved by using the technique of reduced integration. Two point Gaussian quadrature is

used to determine the matrix $\mathbf{K_1}$ while one point Gaussian quadrature is used to find $\mathbf{K_2}$.

The non-linear equations are solved using direct iteration.

2.3 The stream function formulation

Results of the fluid motion are usually interpreted in terms of the stream function ψ, a mathematical construct that relates U and V and ensures that continuity is satisfied identically. The precise relationship between ψ, U and V is

$$U = \frac{\partial \psi}{\partial Y} \quad V = -\frac{\partial \psi}{\partial X}.$$

By differentiating U and V with respect to Y and X respectively and adding the derivatives together, a single equation for the stream function is obtained (see Basak et al.[5]):

$$\frac{\partial^2 \psi}{\partial X^2} + \frac{\partial^2 \psi}{\partial Y^2} = \frac{\partial U}{\partial Y} - \frac{\partial V}{\partial X}. \tag{2.48}$$

We then expand the stream function in the same way as we did U,V and θ to obtain

$$\sum_{j=1}^{361} \psi_j \int_\Omega \left[\frac{\partial \phi_i}{\partial X}\frac{\partial \phi_j}{\partial X} + \frac{\partial \phi_i}{\partial Y}\frac{\partial \phi_j}{\partial Y} \right] dXdY + \sum_{j=1}^{361} U_j \int_\Omega \phi_i \frac{\partial \phi_j}{\partial Y} dXdY - \sum_{j=1}^{361} V_j \int_\Omega \phi_i \frac{\partial \phi_j}{\partial X}\, dXdY = 0. \tag{2.49}$$

The no slip boundary condition is used at all the boundaries and so $\psi = 0$ on all the boundaries. A negative stream function value denotes clockwise flow while a positive

value denotes anti-clockwise flow.

2.4 The Nusselt number

The Nusselt number is the ratio of conductive to convective heat transfer across the boundary and is a measure of heat transfer at the wall. The Nusselt number is dependent on the geometrical and thermal properties of the fluid and on the fluid flow (Heldman [23], Rao [37]). The transfer of heat between a solid surface and the surrounding fluid takes place by a combination of convection and conduction. If the wall of the cavity is at a higher temperature than the surrounding fluid, the heat flows first by conduction to the fluid particles adjacent to the wall. These heated fluid particles are then carried away by flowing fluid to areas of the cavity at a lower temperature.

Within the cavity, either a hot surface is cooled by a cold fluid stream or a cool surface is warmed by a hot fluid stream. Assuming that a hot surface is cooled by a cold fluid stream, the heat from the hot surface would be diffused through a boundary layer and transported away via convection of the cold fluid stream. This process of heat transfer is described by Newton's law of cooling, and is defined as

$$h(T_w - T_f) = -k\frac{\partial T}{\partial \mathbf{n}}, \tag{2.50}$$

where h is the heat transfer coefficient, k is the average thermal conductivity of the fluid, T_w is the temperature at the wall, T_f is the temperature of the fluid away from

the wall and $\mathbf{n}$ is the normal direction to the plane.

When multiplied by L, a characteristic length this gives

$$\frac{hL}{k} = -\frac{1}{T_w - T_f}\frac{\partial T}{\partial \mathbf{n}}L. \tag{2.51}$$

The local Nusselt number is equal to $\frac{hL}{k}$, hence

$$Nu = -\frac{1}{T_w - T_f}\frac{\partial T}{\partial \mathbf{n}}L.$$

In dimensionless form this can be written as:

$$Nu = -\frac{\partial \theta}{\partial \mathbf{n}}d\mathbf{n}. \tag{2.52}$$

The local Nusselt number measures the heat transfer at local points across the cavity. The other concept of interest is that of the average Nusselt number. The average Nusselt number measures the net energy transfer across the length of the cavity wall and is defined as

$$\overline{Nu} = \int_0^1 Nu d\mathbf{n}. \tag{2.53}$$

As previously stated, the Nusselt number is the ratio of conductive to convective heat transfer. For natural convection, the fluid remains stationary with $Nu < 1$. As the Nusselt number increases above 1, fluid motion occurs. In the case of mixed convection, a value below 1 indicates that the heat transfer is due to conduction only. A larger value of the Nusselt number indicates that heat transfer is primarily by convection. The average Nusselt number was calculated using Simpson's 1/3rd rule (Tritton, [46]).

Chapter 3

Results and Discussion

3.1 Streamlines and Isotherms

Much work has been done on mixed convection in a cavity in investigating the effects of heating of various walls of the cavity. This thesis is an extension of work done by Basak et al. [6, 7], who investigated two cases of mixed convection in a square cavity. In the first of these studies, the cavity was uniformly heated from the bottom, while the side walls were cooled with an adiabatic moving lid. In the second study, the cavity was again uniformly heated from the bottom with an adiabatic moving lid, but the side walls were now linearly heated. To extend their work, in this investigation the adiabatic moving lid was replaced with a sinusoidally heated horizontally moving lid for both studies and results were compared.

As stated in Chapter 2, results were found for 20×20 quadratic elements with 361

inner nodes. Results have been found for $Pr = 0.7$ (the value for air), $10^3 \leq Gr \leq 10^5$ and $Re = 1$, 10 and 100.

Benchmark results were found for uniformly heated bottom wall and cooled side walls with an adiabatic stationary lid for $Pr = 0.7$ and $10^3 \leq Ra \leq 10^5$. The results were found to be in good agreement with results in the literature, particularly Basak et al. [5]. Fig 3.1 shows the stream function and temperature contours for the benchmark results.

Figures 3.2 - 3.4 show the results for the stream function and temperature contours for a moving sinusoidally heated lid with linearly heated side walls and uniformly heated bottom wall for $Pr = 0.7$, $Re = 1$, 10 and 100 and a range of Grashof numbers between 10^3 and 10^5.

In Figure 3.2 it can be seen that for $Re = 1$, $Gr = 10^3$, two counter rotating circulations are formed in the cavity. The circulation on the left hand side of the cavity is counter-clockwise while the circulation on the right hand side of the cavity is clockwise. The clockwise flow is significantly stronger than the anti-clockwise flow and thus it can be observed that the flow is dominated by forced convection due to the moving lid. As was expected, the isotherms for $Re = 1$, $Gr = 10^3$ reach a maximum along the bottom wall and at the centre of the top wall, while reaching a minimum at the top corners of the cavity. At the bottom of the cavity, isotherms span the entire width of the cavity. When $\theta \leq 0.6$, the isotherms instead curve upwards towards the lid of the cavity. Hot isotherms at the top of the cavity are restricted to the centre

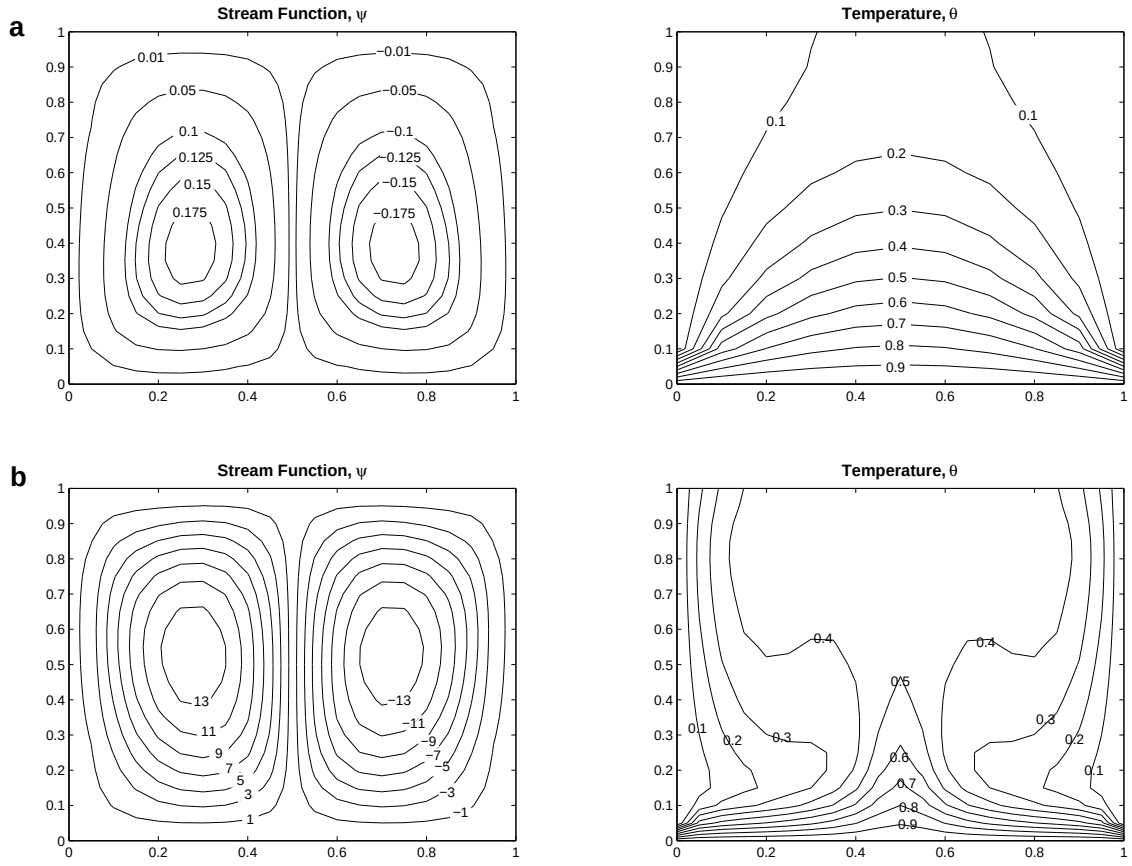

Figure 3.1: Benchmark results for natural convection in a square cavity with uniformly heated bottom wall with $\mathrm{Pr} = 0.7, Re = 1,\ (a)\ Gr = 10^3,\ (b)\ Gr = 10^5$. These results are in good agreement with those of Basak et al. [5].

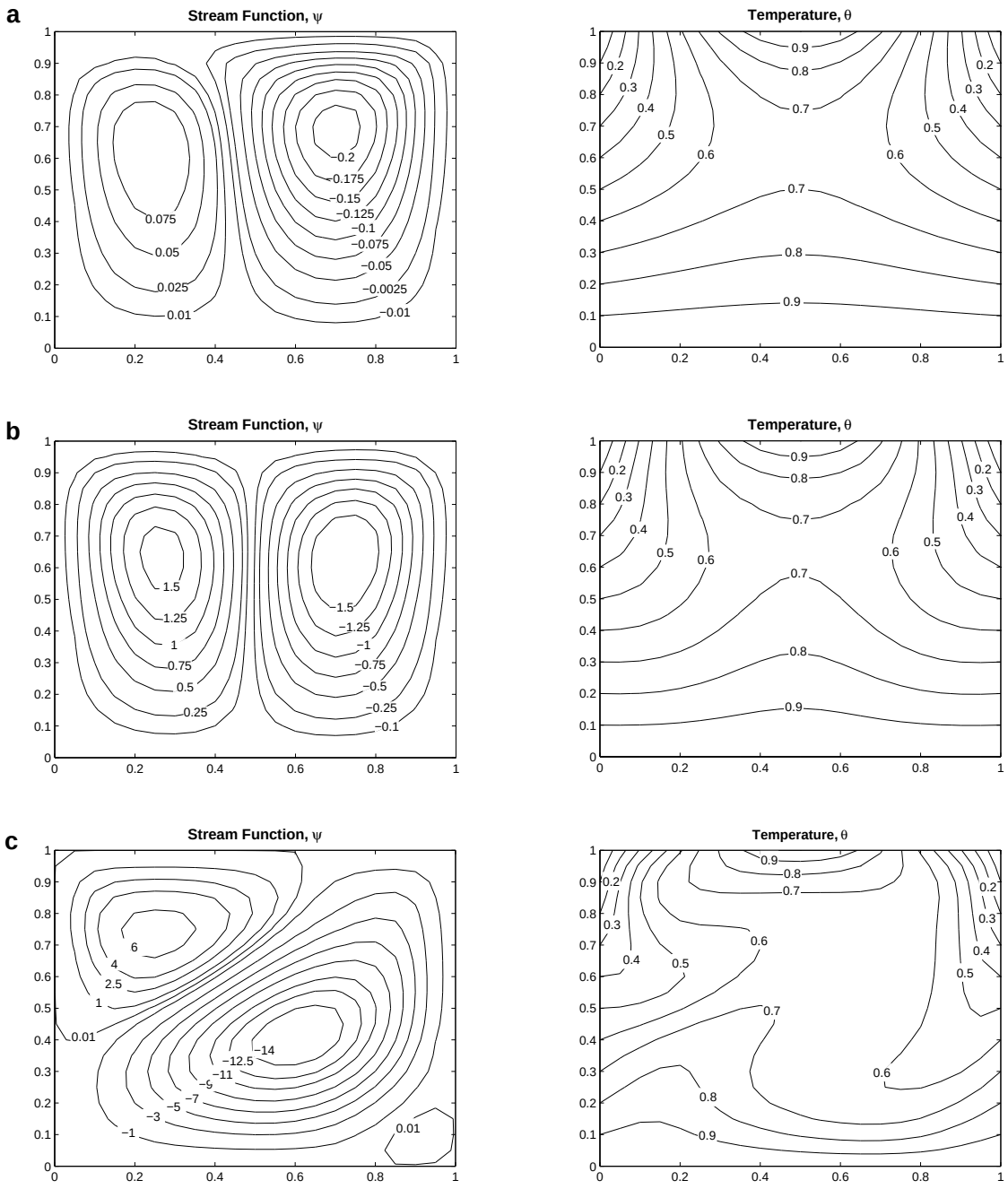

Figure 3.2: Stream function and temperature contours for linearly heated side walls with $\mathrm{Pr} = 0.7, Re = 1,\ (a)\ Gr = 10^3,\ (b)\ Gr = 10^4,\ (c)\ Gr = 10^5$

of the top wall.

As Gr increases to 10^4, it can be observed that the anti-clockwise circulation increases in size and in strength so that two symmetric rotations are formed within the cavity. Natural convection is now as equally dominant as the forced convection regime. The isotherm pattern is similar to that of $Gr = 10^3$, although the heat from the bottom wall has risen slightly higher into the middle of the cavity.

At $Gr = 10^5$, the clockwise circulation in the cavity increases in size and dominates most of the cavity. The circulation is slanted towards the top right and bottom left corners. A small third anti-clockwise circulation is formed at the bottom right hand side of the cavity. It can be seen that the isotherms are compressed in the top corners of the cavity and in the middle of the bottom wall. The isotherms are widely dispersed in the left hand corner of the cavity. This is due to the shape and angle of the clockwise circulation. Cool fluid is brought down on the right hand side of the cavity, while hot fluid is transported upwards towards the middle of the cavity on the left hand side of the bottom wall.

It can be seen that as the Grashof number increases, the strength of the circulations increase as seen in Tables 3.1 and 3.2.

In Figure 3.3 it can be seen that for $Re = 10$ and $Gr = 10^3$, the flow in the cavity is clearly dominated by forced convection. Only a very small secondary circulation is found for this low Grashof number. The isotherms are no longer perfectly symmetrical, but still have a similar shape to that when $Re = 1$.

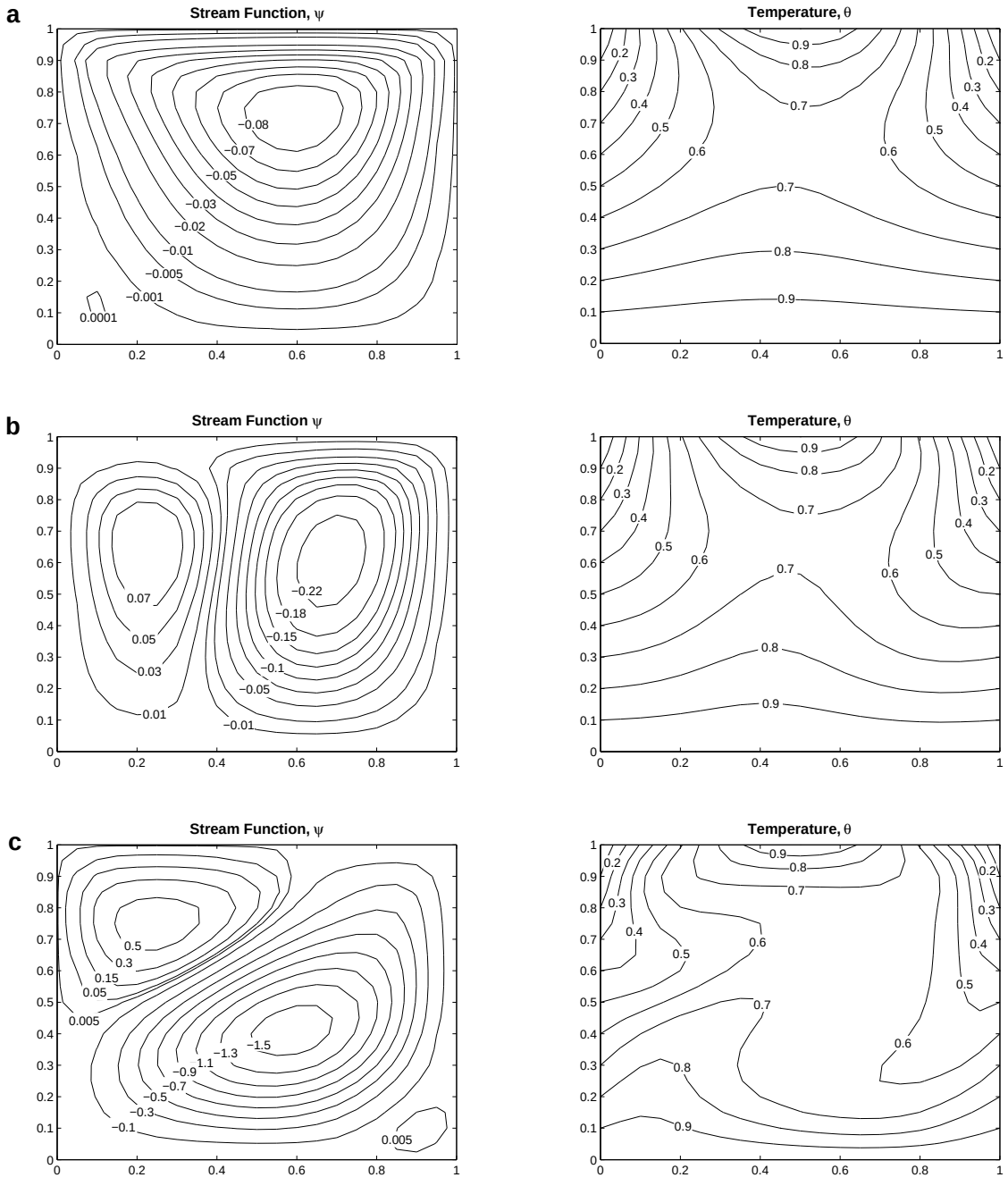

Figure 3.3: Stream function and temperature contours for linearly heated side walls with $\Pr = 0.7, Re = 10,\ (a)\ Gr = 10^3,\ (b)\ Gr = 10^4,\ (c)\ Gr = 10^5$

As Gr increases to 10^4, the secondary circulation on the left hand side of the cavity grows in size and strength. The strength of the clockwise circulation is stronger than that of the anti-clockwise circulation. The flow is still dominated by lid driven flow, but natural convection now has more of an effect on the flow. Again, an increase in the Grashof number causes the heat to rise further towards the centre of the cavity.

Just as when $Re = 1$, at $Gr = 10^5$, the secondary circulation increases in size, becomes slanted and dominates most of the cavity and a small third clockwise circulation is formed at the bottom right hand side of the cavity. The isotherms at $Gr = 10^5$ are also similar in shape to that when $Re = 1$.

In Figure 3.4 at $Re = 100$, $Gr = 10^3$ and $Gr = 10^4$, the flow is again dominated by forced convection. A single clockwise circulation is formed due to strong inertial effects at the top wall. There is little change in the flow as the Grashof number increases from 10^3 to 10^4. From Table 3.2 it can be seen that the centre of the circulation moves down slightly from $Gr = 10^3$ to $Gr = 10^4$ and the circulation is very slightly stronger for $Gr = 10^4$.

The isotherms for both $Gr = 10^3$ and $Gr = 10^4$ are dispersed on the left hand side of the cavity and are compressed on the right hand side of the cavity. This is due to the domination of the forced convection flow regime.

At $Re = 100$, $Gr = 10^5$, a large slanted clockwise circulation is formed which dominates more of the cavity than the circulations when $Re = 1$ and when $Re = 10$. Again a small third anti-clockwise circulation is formed at the bottom right hand corner of

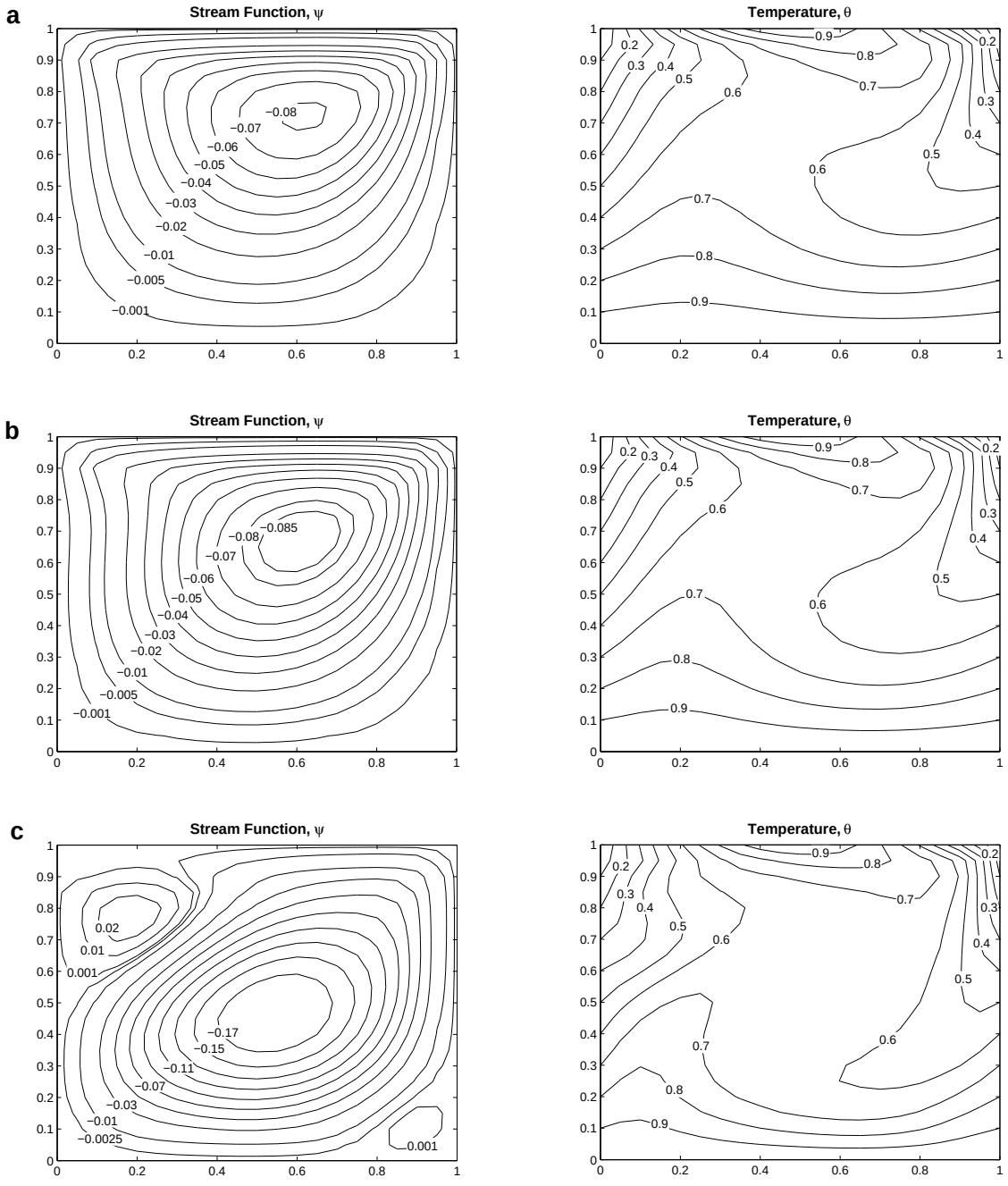

Figure 3.4: Stream function and temperature contours for linearly heated side walls with $\Pr = 0.7, Re = 100,\ (a)\ Gr = 10^3,\ (b)\ Gr = 10^4,\ (c)\ Gr = 10^5$

the cavity. The isotherms are similar in shape for $Re = 1$ and $Re = 10$.

It can be seen that as the Reynolds number increases, the strength of the circulation decreases.

When comparing the results obtained with those from Basak et. al. [6] with an adiabatic top wall, there is a slight difference in the stream function pattern. In general, stream function results found by Basak et. al. [6] are dominated more by forced convection than the present study. For example, their results show that for $Re = 10$, $Gr = 10^3$, a single clockwise circulation is formed within the cavity, while the present results show a small counter-clockwise circulation in the bottom left hand corner of the cavity. As was expected, the temperature contours are very similar in shape to their results at the bottom of the cavity. As the value of y increases, the temperature contours change in shape compared to those of Basak et. al. [6] due to the heating of the top wall.

Figures 3.5-3.7 show the results for the stream function and temperature contours for a moving sinusoidally heated lid with cooled side walls and uniformly heated bottom wall for $Pr = 0.7$, $Re = 1$, 10 and 100 and a range of Grashof numbers between 10^3 and 10^5.

In Figure 3.5 it can be seen that for $Re = 1$ and $Gr = 10^3$, the flow is slightly dominated by forced convection. Two counter rotating circulations are formed in the cavity, with the clockwise circulation being only slightly stronger than anti-clockwise circulation. From Table 3.3 and Table 3.4 it can be seen that for $Gr = 10^3$, the

Table 3.1: Location and value of centre of anti-clockwise circulation for linearly heated side walls

Re	Gr	ψ	x-value	y-value
1	10^3	0.10514	0.25	0.65
1	10^4	1.63131	0.25	0.65
1	10^5	7.03928	0.25	0.75
10	10^3	0.00013	0.1	0.15
10	10^4	0.09818	0.25	0.65
10	10^5	0.63842	0.25	0.75
100	10^3	0	n/a	n/a
100	10^4	0	n/a	n/a
100	10^5	0.02753	0.15	0.75

Table 3.2: Location and value of centre of clockwise circulation for linearly heated side walls

Re	Gr	ψ	x-value	y-value
1	10^3	-0.21528	0.7	0.7
1	10^4	-1.77113	0.75	0.7
1	10^5	-15.50563	0.6	0.4
10	10^3	-0.08987	0.6	0.75
10	10^4	-0.25071	0.7	0.6
10	10^5	-1.61388	0.6	0.4
100	10^3	-0.08150	0.6	0.7
100	10^4	-0.09053	0.6	0.65
100	10^5	-0.19167	0.55	0.45

centre of the anti-clockwise circulation is slightly lower than that of the clockwise circulation. The temperature distribution across the cavity shows that the cavity is at a high temperature across the bottom of the cavity and towards the centre of the top of the cavity. The cavity is cooler towards the side walls and top corners as was expected. The hot isotherms still span the width of the cavity, but are pushed downwards in the corners. For $\theta \geq 0.5$, the isotherms are horizontal across the cavity, but for $\theta \leq 0.4$, the isotherms stretch vertically across the cavity. The temperature distribution obviously differs from that of the linearly heated walls at the side walls. It can also be seen that the contour lines are more widely dispersed towards the bottom of the cavity for the linearly heated case.

As Gr increases to 10^4, the clockwise circulation increases in size to form two counter rotating circulations of a similar size and the natural convection is almost equally dominant to that of forced convection. The centre of the circulations are now at the same height. The temperature contours become slightly more compressed towards the side walls as the Grashof number increases. The hotter contour lines from the top wall are seen to be wider than that of $Gr = 10^3$ and are found to be narrower in the centre towards the bottom wall.

As Gr increases to 10^5, the strength of the stream function increases and the size and position of the two circulations are identical. It can be seen that the hot contour lines have widened even further along the top wall causing the cooler contour lines to become compressed towards the top of the cavity. Towards the bottom of the cavity,

the cool isotherms (those where $\theta \leq 0.4$) are widely dispersed towards the centre of the cavity while the warmer isotherms are compressed towards the bottom wall. This is particularly the case towards the bottom corners of the cavity.

In Figure 3.6 it is clear that for $Re = 10$, $Gr = 10^3$, the flow is dominated by forced convection. The majority of the cavity is dominated by a clockwise rotating circulation. A small anti-clockwise circulation is formed at the bottom left hand side of the cavity. The temperature contours are very similar to the case where $Re = 1$. On close inspection it can be seen that the contours are very slightly more compressed towards the top right corner than when $Re = 1$.

As Gr increases to 10^4, the anti-clockwise circulation grows in size although the clockwise rotating circulation is still larger in size and in strength indicating that the flow is still slightly dominated by forced convection. Again the contour lines are very similar in shape to that of $Re = 1$ and again a slight compression towards the top right hand corner can be seen.

As Gr increases further to 10^5, natural convection becomes equal to forced convection. There is no observable difference in the shape of the temperature contours from that of $Re = 1$.

In Figure 3.7 it can be seen that for $Re = 100$ and $Gr = 10^3$ and $Gr = 10^4$, the fluid flow is dominated by forced convection. For $Gr = 10^3$, only one clockwise rotating circulation appears in the cavity. As Gr increases to 10^4, a small anti-clockwise circulation is formed in the bottom left hand corner of the cavity. As Gr increases

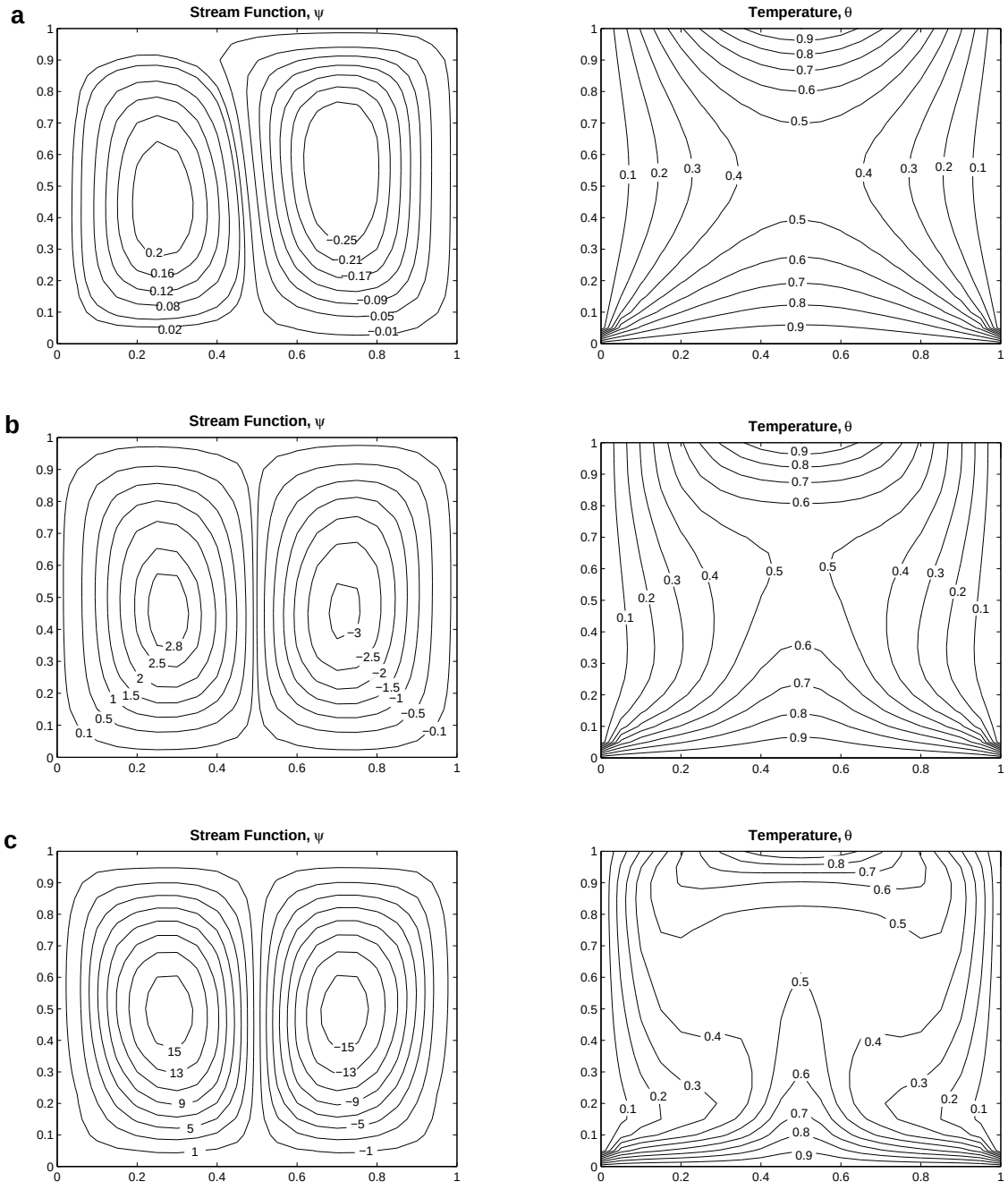

Figure 3.5: Stream function and temperature contours for cooled side walls with $\mathrm{Pr} = 0.7, Re = 1,\ (a)\ Gr = 10^3,\ (b)\ Gr = 10^4,\ (c)\ Gr = 10^5$

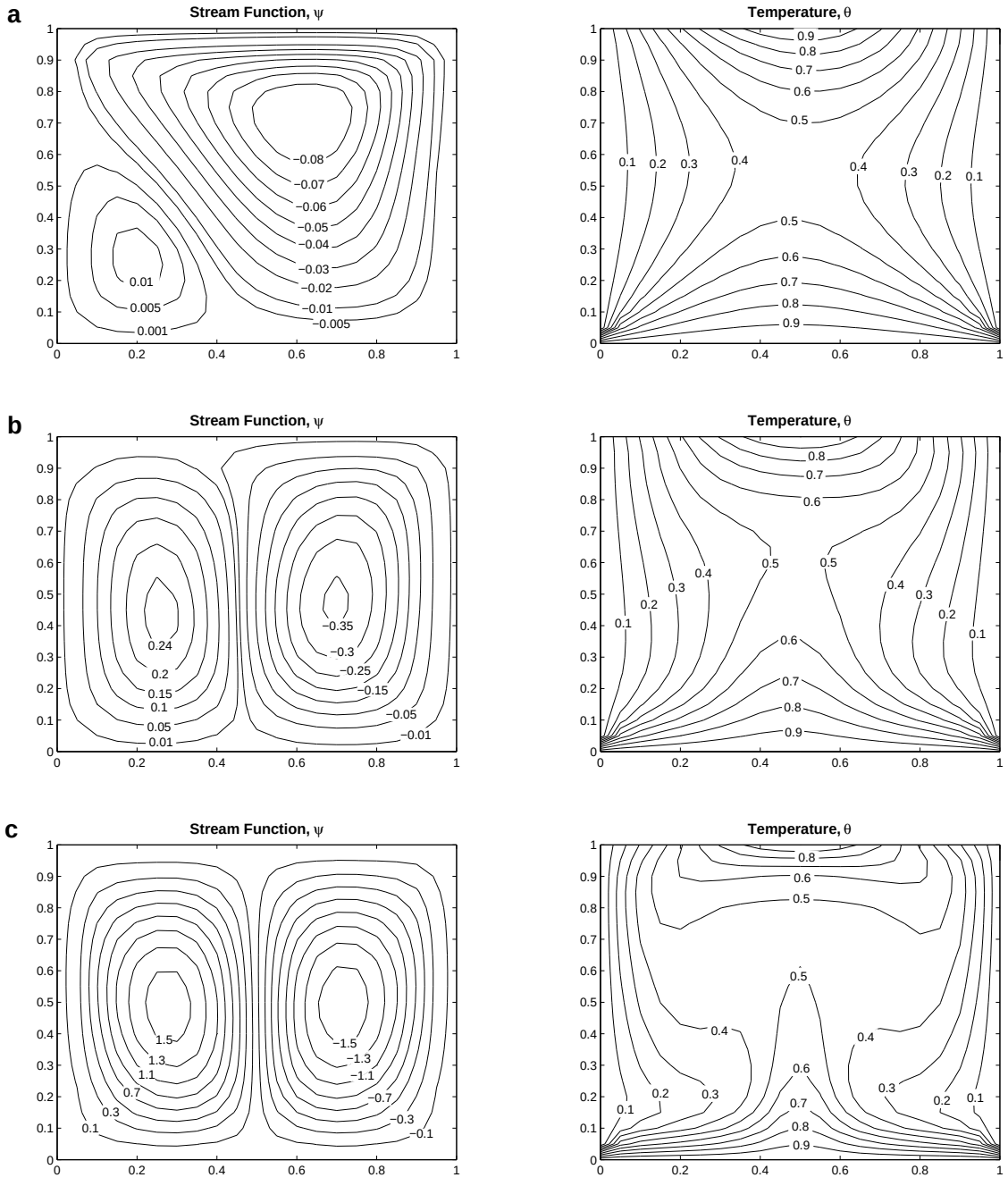

Figure 3.6: Stream function and temperature contours for cooled side walls with $\Pr = 0.7, Re = 10,\ (a)\ Gr = 10^3,\ (b)\ Gr = 10^4,\ (c)\ Gr = 10^5$

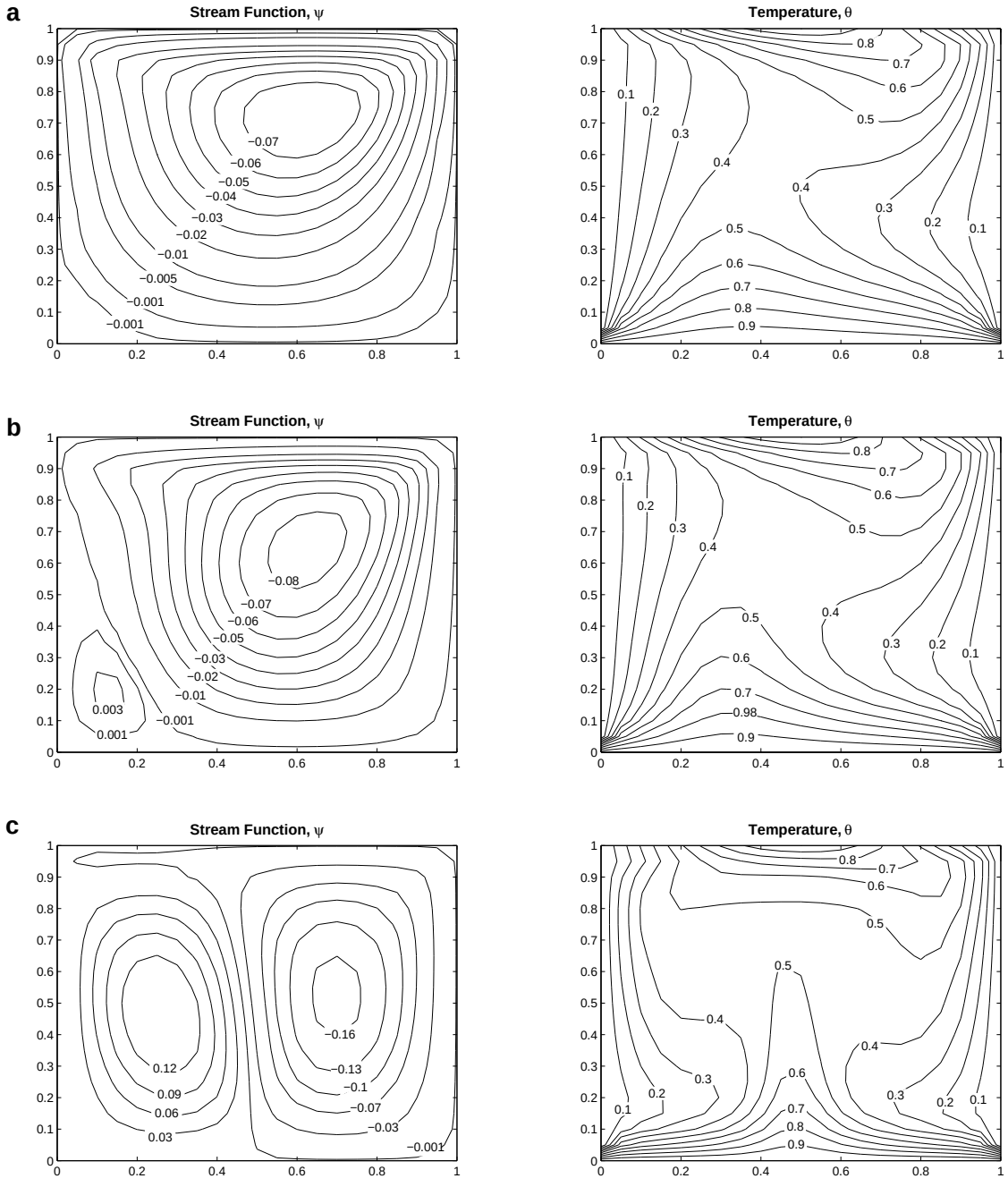

Figure 3.7: Stream function and temperature contours for cooled side walls with $\Pr = 0.7, Re = 100,\ (a)\ Gr = 10^3,\ (b)\ Gr = 10^4,\ (c)\ Gr = 10^5$

to 10^5, the anti-clockwise circulation increases in size and strength. Flow is still slightly dominated by forced convection. The temperature contours for $Re = 100$ show a marked difference to those of $Re = 1$ and $Re = 10$. For $Gr = 10^3$, the hot isotherms (where $\theta \geq 0.5$) are dispersed towards the bottom left and top right corners and compressed in the top left and bottom right corners. The cool isotherms are compressed in the top right and bottom left corners and dispersed towards the centre of the cavity along the middle and bottom of the right wall and at the top of the left wall. The compression and dispersion are more significant along the right side wall than along the left side wall. As Gr increases to 10^4, the hot temperature contours from the bottom wall, move slightly higher towards the centre of the cavity, while the basic shape of the contours remains the same as that of $Gr = 10^3$. A further increase in Gr to 10^5, causes the temperature contours to become compressed in the top two corners of the cavity and more dispersed in the bottom two corners. There is a significant compression of isotherms towards the top right hand corner. The hot temperature contours from the bottom wall become more elongated and extend further towards the centre of the cavity.

It can be observed that in general the circulation is stronger for the case of the cooled side walls than that of the linearly heated walls. Generally, the anti-clockwise circulation is significantly stronger for the cooled walls than the linearly heated walls while the clockwise circulation is only slightly stronger for the cooled walls. For $Gr = 10^3$ and 10^4, the shape of the stream function is very similar between the cooled

Table 3.3: Location and value of centre of anti-clockwise circulation for cooled side walls

Re	Gr	ψ	x-value	y-value
1	10^3	0.23793	0.25	0.45
1	10^4	3.00639	0.3	0.45
1	10^5	16.14951	0.3	0.5
10	10^3	0.01111	0.2	0.25
10	10^4	0.25577	0.25	0.45
10	10^5	1.60625	0.3	0.5
100	10^3	0	n/a	n/a
100	10^4	0.00359	0.15	0.2
100	10^5	0.15368	0.25	0.45

Table 3.4: Location and value of centre of clockwise circulation for cooled side walls

Re	Gr	ψ	x-value	y-value
1	10^3	-0.30927	0.7	0.55
1	10^4	-3.12548	0.7	0.45
1	10^5	-16.16816	0.7	0.5
10	10^3	-0.09203	0.7	0.45
10	10^4	-0.36146	0.7	0.5
10	10^5	-1.62494	0.6	0.4
100	10^3	-0.08062	0.6	0.7
100	10^4	-0.08576	0.65	0.65
100	10^5	-0.17065	0.7	0.5

and heated walls. However, when Gr increases to 10^5, the flow patterns differ greatly. For $Re = 1$ and 10, the cool walls produce two identical counter rotating circulations in contrast to the three tilted circulations resulting from the linearly heated walls. For $Gr = 10^5$, the stream function pattern for the cooled walls shows a slightly stronger clockwise circulation indicating a slight domination by forced convection, but again the flow pattern is very different to that of the linearly heated side walls.

In general, the streamline patters for cooled walls are very similar to that of Basak et al. [6]. Again the temperature contours are similar at the bottom of the cavity, but towards the top of the cavity, the sinusoidally heated top wall changes the temperature contours.

3.2 Heat transfer at the walls

Figure 3.8 shows the effect of the Grashof number on the heat transfer at each of the walls in the cavity for the case of linearly heated side walls.

For all values of the Grashof number, the local Nusselt number is equal to one at the edge of the bottom wall on both sides due to the linear heating of the side walls. For $Gr = 10^3$, the local Nusselt number falls below 1 and reaches a local minimum between $x = 0.4$ and $x = 0.5$. There is not much variation in the Nusselt number across the cavity due to the relatively flat isotherms at the bottom of the cavity.

For $Gr = 10^4$, the Nusselt number is of a similar value to that of $Gr = 10^3$ between

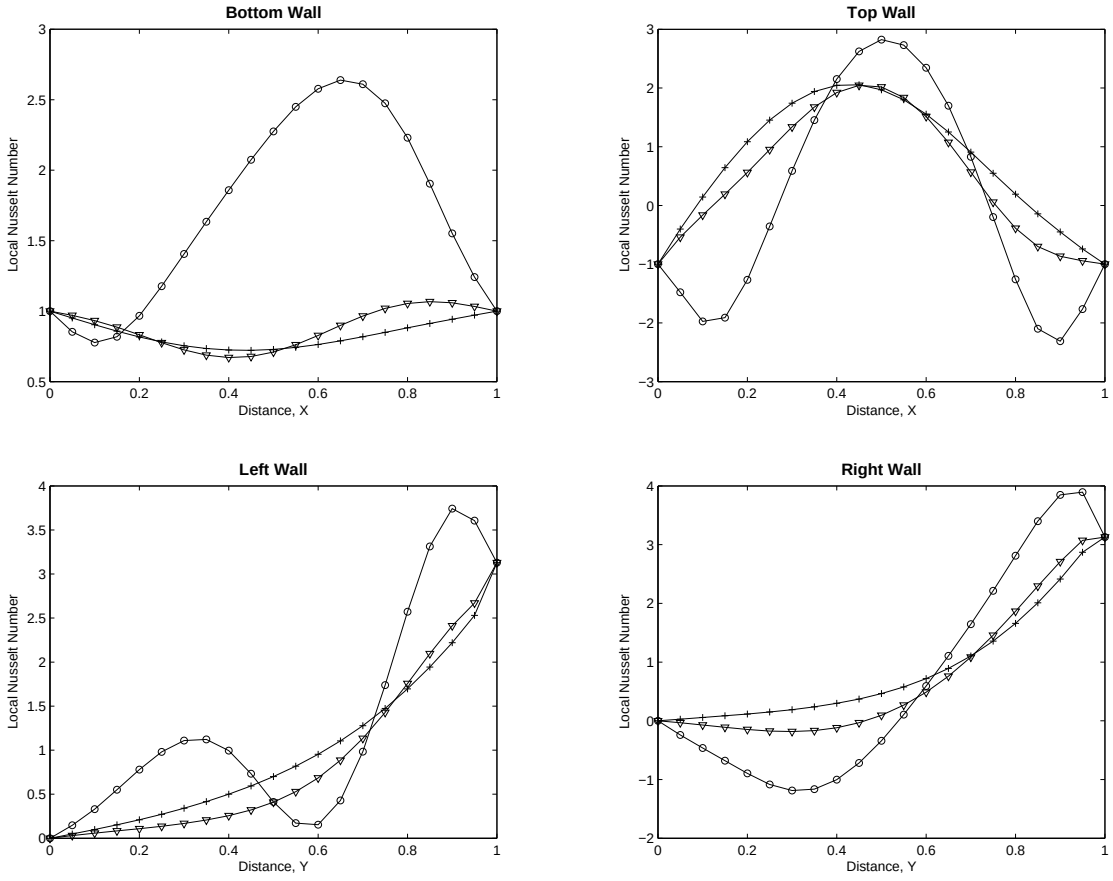

Figure 3.8: Local Nusselt number for linearly heated side walls with $Re = 10$ and $Gr = 10^3$ (+), $Gr = 10^4$ ($\triangle$)andGr=10^5 (o)

$x = 0$ and $x = 0.5$, although the graph falls slightly below that the graph when $Gr = 10^3$ near $x = 0.4$ reaching a local minimum here. After $x = 0.6$ the graph rises above that of $Gr = 10^3$, reaching a maximum at $x = 0.8$.

For $Gr = 10^5$, the Nusselt number is greater than 1 for the majority of the cavity due to the compressed isotherms. The Nusselt number drops below 1 between $x = 0$ and $x = 0.2$ due to the widely dispersed isotherms on the left hand side of the cavity. The Nusselt number is at a maximum at $x = 0.7$.

The local Nusselt number at the bottom wall is very similar in shape to that of Basak et al. [6] since the the temperature contours are very similar between the two studies at the bottom of the cavity.

The local Nusselt number at the edges of the top wall is equal to -1 for all values of the Grashof Number due to the linearly heated walls. For $Gr = 10^3$ the Nusselt number rises and reaches a local maximum at $x = 0.4$ and then gradually decreases. For $Gr = 10^4$, the Nusselt number follows a similar pattern to that of $Gr = 10^3$, although is lower than the graph of $Gr = 10^3$. At $Gr = 10^5$, the graph of the Nusselt number is close to being symmetric in shape. The Nusselt number drops to a local minimum at $x = 0.1$ and then rises to a local maximum at the centre of the cavity. The Nusselt number then drops again to a local minimum at $x = 0.9$.

Since the top wall is adiabatic in the study by Basak et al. [6] and therefore the heat transfer is zero at the wall, it is not possible to make a comparison between the two studies at the top wall.

For $Gr = 10^3$, the local Nusselt number at the right hand wall gradually increases as y increases up the cavity. For $Gr = 10^4$, a similar occurrence happens, although the Nusselt number is below that of $Gr = 10^3$ until $y = 0.8$ where the Nusselt number becomes greater than that of $Gr = 10^3$. For $Gr = 10^5$, the Nusselt number decreases below 0 attaining a local minimum at $y = 0.3$ due to the compressed isotherms at the bottom corner of the right wall. The Nusselt number then increases reaching a local maximum at $y = 0.9$.

The shape of the graph is similar to that of Basak et al. [6] especially towards the bottom of the cavity. Towards the top of the cavity, the slope of the graph for Basak et al. [6] becomes quite steep whereas the graph for this studies becomes level towards the end and in the case of $Gr = 10^5$, decreases at the top of the cavity. This is due to the difference in the adiabatic and sinusoidally heated top wall.

The local Nusselt number at the left hand wall for $Gr = 10^3$ and $Gr = 10^4$ is very similar in shape to that of the right hand wall due to a near symmetrical isotherm pattern at the two walls. However at $Gr = 10^5$, the local Nusselt number at the left hand wall is above 0 for the entire height of the cavity and has an oscillatory pattern. The Nusselt number initially rises attaining a local maximum at $y = 0.3$ due to the dispersed isotherms along the bottom half of the left hand wall. The Nusselt number then drops as the isotherms compress and reaches a local minimum at $y = 0.6$. Towards the top of the cavity the isotherms become more dispersed once again and the Nusselt number again rises to a local maximum at $y = 0.9$.

The graph at the left hand wall is similar in shape for $Gr = 10^3$ to that of Basak et al.[6]. For $Gr = 10^5$, the graph of Basak et al. [6] also exhibits a slightly oscillatory shape. However, as with the right wall, the graph in the present study has a local maximum near the top corner and then decreases again as opposed to the graph from Basak et al. which increases to the wall. Again this is due to the difference between the adiabatic and heated lid.

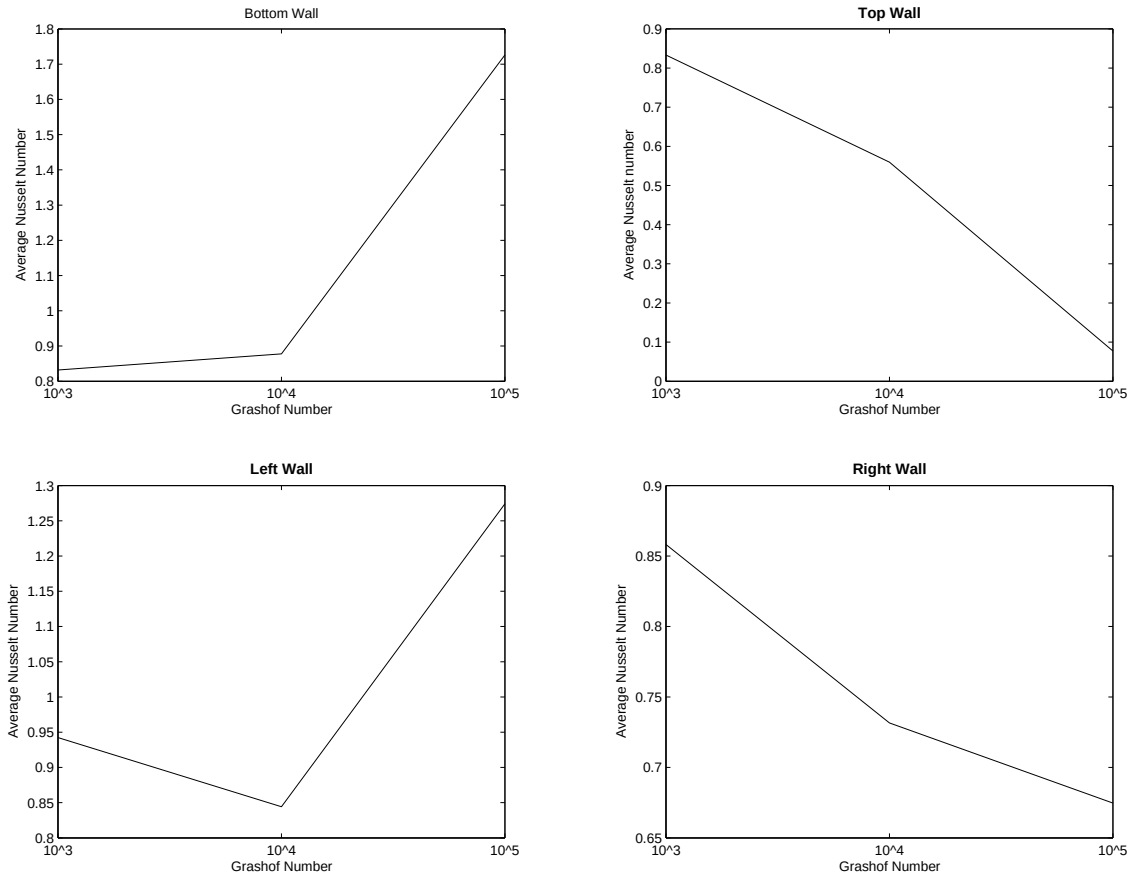

Figure 3.9: Average Nusselt number for linearly heated side walls with Re=10

Figure 3.9 shows the average Nusselt number at the four walls of the cavity. The graphs are not smooth since the average Nusselt number has only been calculated at

$Gr = 10^3$, $Gr = 10^4$ and $Gr = 10^5$. At the bottom wall, the Nusselt Number is seen to increase as the Grashof number increases. The graph of average Nusselt number at the bottom wall is almost identical to the results of Basak et al. [6]. At the top wall, the opposite is seen to happen. As the Grashof number increases, the isotherms become more compressed in the top corners. At the left hand side wall, the average Nusselt number is lower for $Gr = 10^4$ than it is for $Gr = 10^3$. This is due to the slight dip in the isotherms at the left wall. The average Nusselt number at the left wall then increases for $Gr = 10^5$. The average Nusselt number at the right side wall decreases as the Grashof number increases. Again this is due to a slight dip in the isotherms at the right wall for $Gr = 10^4$ and a significant compression of isotherms towards the bottom corner for $Gr = 10^5$. Although the local Nusselt number is higher than $Gr = 10^3$ and $Gr = 10^4$ at the top of the right wall, this significant compression at the bottom causes the average Nusselt number of $Gr = 10^5$ to fall below that of the lower Grashof numbers.

The local Nusselt number at the bottom wall for cooled side walls is shown in Figure 3.10. For all values of the Grashof number, the Nusselt number decreases to $x = 0.5$ where it obtains a local minimum and then increases again towards the right hand side of the cavity. Along most of the cavity, the local Nusselt number for $Gr = 10^3$ is lower than that of $Gr = 10^4$ which in turn is lower than that of $Gr = 10^5$. Basak et al. [7] only show local Nusselt number results for $Gr = 10^4$. The Nusselt number graph at the bottom wall is almost identical between the two studies.

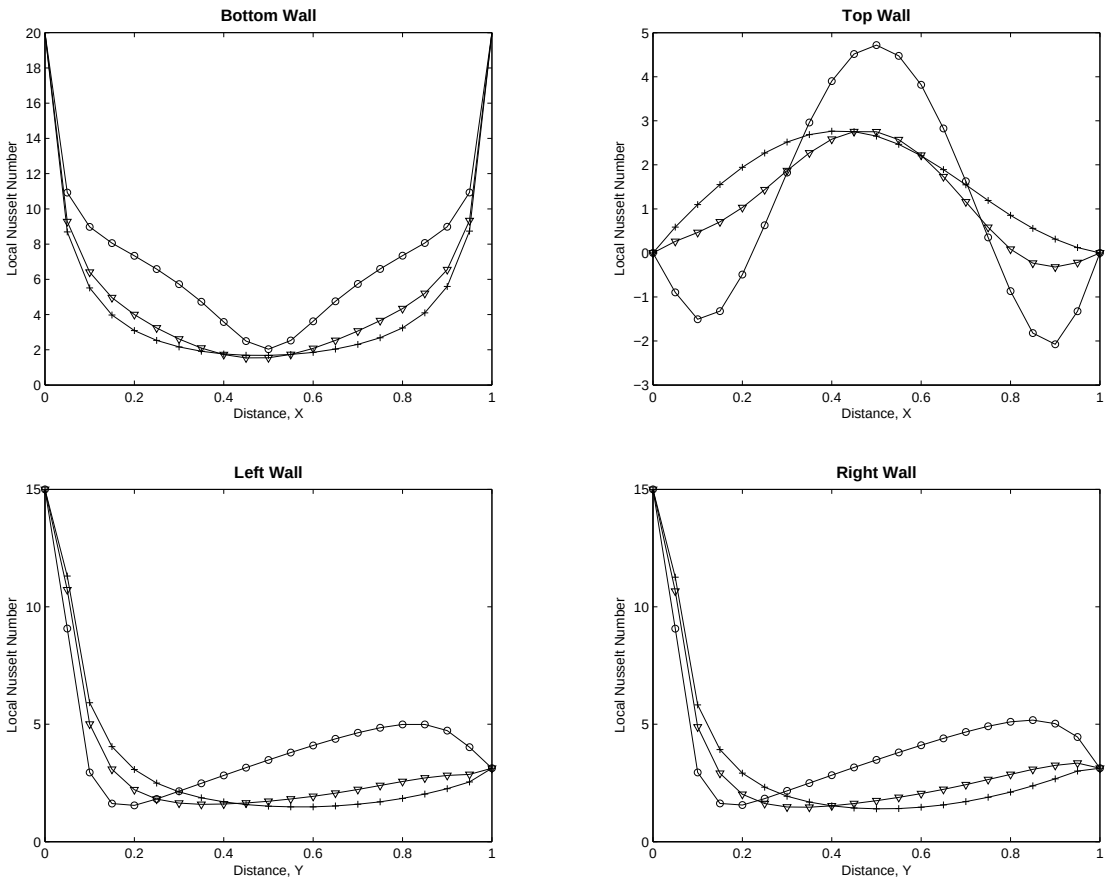

Figure 3.10: Local Nusselt number for cooled side walls with $Re = 10$, $Gr = 10^3(+)$, $Gr = 10^4(\triangle)$ and Gr=10^5(o)

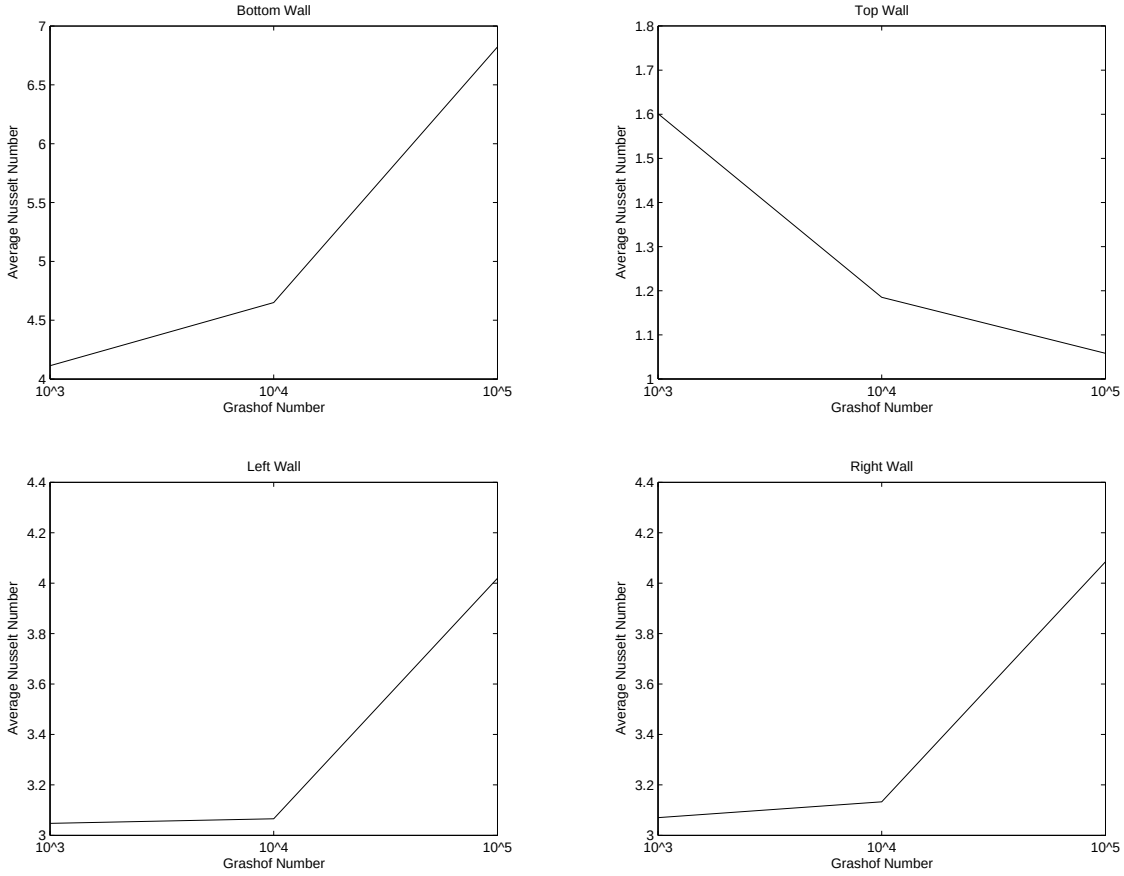

Figure 3.11: Average Nusselt number for cooled side walls

In contrast to the case for linearly heated side walls, the local Nusselt number at the bottom wall for cooled walls is concave up since the isotherms are equal to 0 at the corners of the bottom wall for the cooled walls.

The graphs of the local Nusselt number at the left and right walls are almost symmetrical due to the symmetry of the isotherms across the cavity. At both walls, the local Nusselt number decreases to a local minimum at $y = 0.6$ for $Gr = 10^3$ and then increases slightly towards the top of the cavity. For $Gr = 10^4$, the Nusselt number decreases to a local minimum near $y = 0.3$ and then slowly increases towards the top of the cavity. The local Nusselt number for $Gr = 10^4$ is below that of $Gr = 10^3$ until $y = 0.45$ where it increases above that of $Gr = 10^3$ due to a slightly larger compression of the isotherms above $y = 0.45$. For $Gr = 10^5$, the local Nusselt number decreases to a local minimum near $y = 0.2$ due to the dispersion of isotherms near the bottom corner(s). The Nusselt number then increases above that of $Gr = 10^4$ and $Gr = 10^3$ at $y = 0.25$ and $y = 0.3$ respectively due to the more compressed isotherms in the top corners. The Nusselt number then increases to a local maximum near $y = 0.8$ and decreases slightly to the top of the cavity. There is no oscillatory pattern for $Gr = 10^5$ which was observed in the case of the heated side walls. This is due to the to the difference in the temperature distributions.

The graphs at the left and right walls for cooled side walls are in contrast to the case for heated walls, where the left and right side walls exhibit a largely different local Nusselt number graph especially for the case of $Gr = 10^5$ since for cooled walls the

isotherms are almost symmetrical while for the case of linearly heated side walls, the isotherms are obviously unsymmetrical for $Gr = 10^5$.

The shape of the Nusselt number at the right wall is similar to that of Basak et al. [7]. However, the graph of the Nusselt number at the left wall for the study by Basak et al. is slightly different. In this study the Nusselt number decreases and then increases slightly, while for Basak et al. [7] the Nusselt number decreases across the length of the cavity. This is due to the fact that Basak's isotherms at the top left hand side of the cavity are widely dispersed, while in this case the sinusoidal heating of the top wall prevents the cooler isotherms from becoming dispersed.

The local Nusselt number at the top wall is equal to 0 on either side of the cavity due to the cool side walls. The shape is similar to the case of linearly heated side walls although the value of the local Nusselt number is higher across the cavity for the case of cooled side walls.

For $Gr = 10^3$, the local Nusselt number increases to a local maximum at $x = 0.4$ and then decreases again to 0 at the right side wall. For $Gr = 10^4$, the local Nusselt number is below that of $Gr = 10^3$ across the majority of the cavity. The Nusselt number increases to a local maximum at $x = 0.5$ and decreases to at the right side of the cavity.

For $Gr = 10^5$, the Nusselt number decreases below 0 to reach a local minimum at $x = 0.1$. The Nusselt number then increases along the cavity to a local maximum at $x = 0.5$. It then decreases again to a local minimum $x = 0.9$, which is slightly lower

than the minimum at $x = 0.1$, and then increases to 0 at the right side wall.

Chapter 4

Conclusion

A numerical study has been performed using the Penalty Galerkin Finite Element method to analyse mixed convective heat transfer and fluid flow in an air filled square cavity. The aim of this study was two-fold. Firstly we aimed to extend the research done by Basak et al. [6, 7] to include a sinusoidally heated lid instead of an adiabatic lid and compare the results. Secondly we aimed to compare the differences in results found for linearly heated side walls and uniformly cooled side walls.

For the case of linearly heated side walls it was found that;

- The fluid flow exhibited a similar behaviour to that of Basak et al. [6]. However, in general, the flow in this investigation was dominated more by natural convection than in the previous study.
- Temperature contours were similar at the bottom wall, but differed towards the top of the cavity due to the effect of the sinusoidally heated top wall.

- The local Nusselt Number is very similar to that of Basak et al. [6] at the bottom wall and at the bottom sections of the left and right walls. However, at the top of the side walls, the Nusselt numbers for Basak et al. [6] continue increasing while the sinusoidally heated top wall causes the Nusselt number to decrease at the top of the cavity for $Gr = 10^5$ and to level out for lower Grashof numbers.

For the case of cooled side walls it was found that;

- The fluid flow pattern was almost identical to that of Basak et al. [7].
- As was the case with heated side walls, the temperature profiles were similar at the bottom of the cavity, but differed towards the top of the cavity due to the effect of the sinusoidally heated top wall.
- The local Nusselt number is again very similar to that of Basak et al. [7] at the bottom wall and lower portions of the side walls. However towards the top of the cavity, the sinusoidal wall causes the local Nusselt number to rise slightly for both walls in contrast to the adiabatic case where the Nusselt number where it is level towards the top of the cavity at the left wall and continues to decrease at the right wall.

The second part of the current investigation aimed to compare the effects of linearly heated and uniformly cooled walls on fluid flow and temperature profiles. It was observed that;

- In general the strength of circulation was stronger for the case of the cooled walls.

- The anti-clockwise circulation was significantly stronger for cooled walls, while the clockwise circulation was only slightly stronger for the cooled walls and the difference in strength decreased both with increasing Reynolds and Grashof numbers.

- The temperature contours obviously differ along the side walls due to the difference in heating at these walls and differ greatly for $Gr = 10^5$.

- Both the local and average Nusselt numbers are generally higher for the case of cooled side walls than that of heated side walls.

- The local Nusselt Number at the left and right walls are very similar for the case of cooled side walls due to symmetric patterns in the temperature isotherms. However, particularly for $Gr = 10^5$, the heated side walls have very different local Nusselt numbers at the two different walls.

- The local Nusselt number at the top wall is very similar in shape between the two cases although the linearly heated case is lower in value than the cooled side walls.

In future it may be useful to extend this research to include the effects of heat sources of various lengths in one or more of the walls, i.e. heating only half a wall and cooling

the other half or a heat source in the centre of the cavity. Further research could also include the effects of a tilted cavity on fluid flow and heat transfer.

References

[1] J. D. Anderson, The Handbook of Fluid Dynamics, CRC Press, Florida, 1998.

[2] J. E. Akin, Finite Elements for Analysis and Design, Academic Press Limited, London, 1994.

[3] U. M. Ascher, Numerical Methods for Evolutionary Differential Equations, Society for Induistrial and Applied Mathematics, Philadelphia, 2008.

[4] O. Aydin, W. Yang, Natural convection in enclosures with localized heating from below and symmetric cooling from sides, International Journal of Numerical Methods for Heat and Fluid Flow 10 (2000) 518-529.

[5] T. Basak, S. Roy, A. R. Balakrishnan, Effects of thermal boundary conditions on natural convection flows within a square cavity, International Journal of Heat and Mass Transfer 49(2006) 4525-4535.

[6] T. Basak, S. Roy, P. K. Sharma, I. Pop, Analysis of mixed convection flows within a square cavity with linearly heated side wall(s), International Journal of Heat and Mass Transfer 52 (2009) 2224-2242.

[7] T. Basak, S. Roy, P. K. Sharma, I. Pop, Analysis of mixed convection flows within a square cavity with uniform and non-uniform heating of bottom wall, International Journal of Thermal Sciences 48 (2009) 891-912.

[8] G. K. Batchelor, Heat transfer by free convection across a closed cavity between vertical boundaries at different temperatures, Quarterly Journal of Applied Mathematics 12 (1954) 209-226.

[9] E. Bilgen, R. B. Yedder, Natural convection in enclosure with heating and cooling by sinusoidal temperature profiles on one side, International Journal of Heat and Mass Transfer 50 (2007) 139-150.

[10] D. Bresch, B. Desjardins, On the existence of global weak solutions to the Navier-Stokes equations for viscous compressible and heat conducting fluids, Journal de Mathematiques Pures et Appliquees 87 (2007) 57-90.

[11] O. R. Burggraf, Analytical and numerical studies of the structure of steady separated flows, Journal of Fluid Mechanics 24 (1966) 113-151.

[12] B. Calcagni, F. Marsili, M, Paroncini, Natural convective heat transfer in square enclosures heated from below, Applied Thermal Engineering 25 (2005) 2522-2531.

[13] N. Cheikh, B. Beya, T. Lili, Influence of thermal boundary conditions on natural convection in a square enclosure partially heated from below, International Communications in Heat and Mass Transfer 34 (2007) 369-379.

[14] Q. Chen, C. Miao, Z. Zhang, On the uniqueness of weak solutions for the 3D Navier Stokes equations, Ann. I. H. Poincare 26 (2009) 2165-2180.

[15] T. S. Cheng, W. H. Liu, Effect of temperature gradient orientation on the characteristics of mixed convection flow in a lid-driven square cavity, Computers and Fluids 39 (2010) 965-978.

[16] M. Corcione, Effects of the thermal boundary conditions at the sidewalls upon natural convection in rectangular enclosures heated from below and cooled from above, International Journal of Thermal Sciences 42 (2003) 199-208.

[17] M. Das, P. Kanna, Application of an ADI scheme for steady and periodic solutions in a lid-driven cavity problem, International Journal of Numerical Methods for Heat and Fluid Flow 17 (2007) 799-822.

[18] G. De Vahl Davis, Laminar natural convection in an enclosed rectangular cavity, International Journal of Mass Transfer 11 (1968) 1675-1693.

[19] E. G. Eckert, W. O. Carlson, Natural convection in an air layer enclosed between two vertical plates with different temperatures, International Journal of Heat and Mass Transfer 2 (1961) 106-110.

[20] P. M. Gresho, R. L. Sani, Incompressible Flow and the Finite Element Method, Volume 2, Isothermal Laminar Flow, John Wiley and Sons Ltd, Chichester, 1998.

[21] J. C. Heinrich, R. S. Marshall, Viscous Incompressible Flow by a Penalty Function Finite Element Method, Computers and Fluids 9 (1981) 73-83.

[22] K. H. Huebner, D. L. Dewhirst, D. E. Smith, T. G. Byron, The Finite Element Method for Engineers, Fourth Edition, John Wiley and Sons, New York, 2001.

[23] D. R. Heldman, Encyclopedia of agriculture, food and biological engineering, Taylor and Francis, 2003.

[24] A. Iserles, A First Course in the Numerical Analysis of Differential Equations, Cambridge University Press, Cambridge, 2009.

[25] M. Kawaguti, Numerical Solution of the Navier-Stokes equations for the flow in a two-dimensional cavity, Journal of the Physical Society of Japan 16 (1961) 2307-2318.

[26] R. J. Leveque, Finite Volume Methods for Hyperbolic Problems, Cambridge University Press, Cambridge, 2002.

[27] R. S. Marhall, J. C. Heinrich, O. C. Zienkiewicz, Natural Convection in a Square Enclosure by a Finite Element Penalty Function Method using Primitive Fluid Variables, Numerical Heat Transfer 1 (1978) 315-330.

[28] M. Moallemi, K. S. Jang, Prandtl number effects on laminar mixed convection heat transfer in a lid driven cavity, International Journal of Heat and Mass transfer 35(1992) 1881-1892.

[29] N. Nithyadevi, P. Kandaswamy, J. Lee, Natural convection in a rectangular cavity with partially active side walls, International Journal of Heat and Mass Transfer 50 (2007) 4688-4697.

[30] S. Ostrach, Natural Convection in Enclosures, Advances in Heat Transfer 7 (1972) 161-227.

[31] H. Oztop, I. Dagtekin, Mixed convection in two-sided lid-driven differentially heated square cavity, International Journal of Heat and Mass Transfer 47 (2004) 1761-1769.

[32] D. W. Pepper, J. C. Heinrich, The Finite Element Method, Basic Concepts and Applications, Taylor and Francis Group, Florida, 2006.

[33] T. Pesso, S. Piva, Laminar natural convection in a square cavity: Low Prandtl numbers and large density differences, International Journal of Heat and Mass Transfer 52 (2009) 1036-1043.

[34] G. Poots, Heat transfer by laminar free convection in enclosed plan gas layers, Quarterly Journal of Mechanics and Applied Mathematics 11 (1958) 257-273.

[35] Y. S. Prasad, M. K. Das, Hopf bifurcation in mixed convection flow inside a rectangular cavity, International Journal of Heat and Mass Transfer, 50 (2007) 3583-3598.

[36] A. K. Prasad, J. R. Koseff, Combined forced and natural convection heat transfer

in a deep lid-driven cavity flow, International Journal of Heat and Fluid Flow 17 (1996) 460-467.

[37] Y. V. Rao, Heat Transfer, University Press Limited, Hyderbad, India, 2001.

[38] J. N. Reddy, An introduction to Finite Element Analysis, McGraw-Hill, New York, 1993.

[39] I. E. Sarris, I. Lekakis, N. S. Vlachos, Natural convection in a 2d enclosure with sinusoidal upper wall temperature, Numerical Heat Transfer, 42 (2002) 513-530.

[40] M. Sathiyamoorthy, T. Basak, S. Roy, N. C. Mahanti, Effect of the Temperature Difference Aspect Ratio on Natural Convection in a Square Cavity for Nonuniform Thermal Boundary Conditions, Journal of Heat Transfer 129 (2007) 1723-1728.

[41] J. Saleh, Fluid Flow Handbook, McGraw Hill Companies, New York, 2002.

[42] V. Sivakumar, S. Sivasankaran, P. Prakash, J. Lee, Effect of heating location and size on mixed convection in lid-driven cavities, Computers and Mathematics with Applications 59 (2010) 3053-3065

[43] C. Taylor, A. Z. Ijam, A finite element numerical solution of natural convection in enclosed cavities, Computer Methods in Applied Mechanics and Engineering 19 (1979) 429-446.

[44] G. A Tokaty, A History and Philosophy of Fluid Mechanics, Dover Publications, Mineola, New York, 1971.

[45] K. Torrance, R. Davis, K. Eike, P. Gill, D. Gutman, A. Hsui, S. Lyons and H. Zien, Cavity Flows Driven by Buoyancy and Shear, Journal of Fluid Mechanics 51 (1972) 221-231.

[46] D. J. Tritton, Physical Fluid Dynamics, Van Nostrand Reinhold Company Ltd., Berkshire, England, 1977.

[47] http://en.wikipedia.org/wiki/Finite_element_method.

[48] J. C. Wong, Numerical Simulation of two-dimensional laminar mixed-convection in a lid-driven cavity using the mixed finite element consistent splitting scheme, International Journal of Numerical Methods for Heat and Fluid Flow 17 (2007) 46-93.

[49] O.C. Zienkiewicz, Finite Elements and Approximation, Wiley and Sons, New York, 1982.